[18] Hagemans ML, Winkel LP, Van Doorn PA, Loonen MC, Hop WJ, Reuser AJ, et al. Clinical manifestation and natural course of late-onset Pompe's disease in 54 Dutch patients. Brain 2005;128:671–7.
[19] Oskoui M, Levy G, Garland CJ, Gray JM, O'Hagen J, De Vivo DC, et al. The changing natural history of spinal muscular atrophy type 1. Neurology 2007;69: 1931–6.
[20] Sienko Thomas S, Buckon CE, Nicorici A, Bagley A, McDonald CM, Sussman MD. Classification of the gait patterns of boys with Duchenne muscular dystrophy and their relationship to function. J Child Neurol 2010;25:1103–9.
[21] Eisenberg I, Grabov-Nardini G, Hochner H, Korner M, Sadeh M, Bertorini T, et al. Mutations spectrum of GNE in hereditary inclusion body myopathy sparing the quadriceps. Hum Mutat 2003;21:99.

Clinical Neurology and Neurosurgery 114 (2012) 678–683

Contents lists available at SciVerse ScienceDirect

Clinical Neurology and Neurosurgery

journal homepage: www.elsevier.com/locate/clineuro

Case series

Clinicopathological features of centronuclear myopathy in Japanese populations harboring mutations in dynamin 2

Madoka Mori-Yoshimura[a], Aya Okuma[b], Yasushi Oya[a], Chieko Fujimura-Kiyono[c], Hideto Nakajima[c], Keita Matsuura[d], Aya Takemura[a], May Christine V. Malicdan[b], Yukiko K. Hayashi[b], Ikuya Nonaka[b], Miho Murata[a], Ichizo Nishino[b,*]

[a] Department of Neurology, National Center Hospital of Neurology and Psychiatry, 4-1-1 Ogawahigashi-cho, Kodaira, Tokyo 187-8551, Japan
[b] Department of Neuromuscular Research, National Institute of Neuroscience, National Center of Neurology and Psychiatry, 4-1-1 Ogawahigashi-cho, Kodaira, Tokyo 187-8502, Japan
[c] Department of Neurology, Osaka Medical College, Daigaku-Machi 2-7, Takatsuki, Osaka 569-8686, Japan
[d] Department of Neurology, Kinan Hospital 4750, Atawa, Mihama-chou, Minamimuro-gun, Mie 513-8505, Japan

ARTICLE INFO

Article history:
Received 25 October 2010
Received in revised form 26 October 2011
Accepted 30 October 2011
Available online 19 May 2012

Keywords:
Centronuclear myopathy
Dynamin 2
Congenital myopathy
Radial distribution
Clinicopathological homology

ABSTRACT

Background: Missense mutations in dynamin 2 gene (*DNM2*) are associated with autosomal dominant centronuclear myopathy (CNM) with characteristic histopathological findings of centrally located myonuclei in a large number of muscle fibers.
Methods: To identify Japanese CNM caused by *DNM2* mutations (DNM2-CNM), we sequenced *DNM2* in 22 unrelated Japanese patients who were pathologically diagnosed with CNM. The clinical and pathological findings of DNM2-CNM in patients were reviewed.
Results: We identified 3 different heterozygous missense mutations (p.E368K, p.R369W, and p.R465W) in 4 probands from 4 families. Clinically, calf muscle atrophy and *pes cavus* are features that are highly suggestive of DNM2-CNM among all CNMs. Pathologically, all 4 DNM2-CNM patients showed a radial distribution of myofibrils in scattered fibers, type 1 fiber atrophy, type 1 fiber predominance, and type 2C fibers. None of the non-DNM2-CNM patients exhibited all the 4 abovementioned pathological features, although some patients showed radial distribution without type 1 fiber atrophy and/or type 2C fibers.
Discussion: These results indicate that the clinicopathological features of DNM2-CNM are rather homogeneous and can be distinguished from the features of non-DNM2-CNM.

1. Introduction

Centronuclear myopathy (CNM) is a rare congenital myopathy named after its characteristic feature of centrally located nuclei in majority of the muscle fibers [1]. In autosomal dominant (AD) cases, muscular weakness and atrophy often begin in childhood or early adolescence [2,3]. CNM progresses slowly, and patients usually follow a mild course and can often expect a normal life-span. In muscle biopsy, a radial alignment of intermyofibrillar networks [1] is seen in nicotinamide adenosine dinucleotide-tetrazolium reductase (NADH-TR) preparations due to the presence of central nuclei; type 1 fiber atrophy is also often observed. Several families with CNM are found in Europe, the United States, Central Africa, Argentina, and Japan [2–6].

Thus far, 4 causative genes have been reported for CNM: myotubularin (*MTM1*), dynamin 2 (*DNM2*) [7], *hJUMPY* [8], and amphiphysin 2 (*BIN1*) [9]. Among them, *DNM2* mutations have been identified among patients in France, French Guiana, the United States, Belgium, Germany, Great Britain, Argentina, and Central Africa [6,10,11]. *DNM2* encodes a protein involved in endocytosis, membrane trafficking, actin assembly, and centrosome cohesion [12–14]. Thus, *DNM2* mutations cause a reduction of dynamin in transfected fibroblasts, leading to defects in centrosomal function.

Patients with CNM that is caused by mutation in the middle domain of *DNM2* (DNM2-CNM) present with a homogenous mild phenotype characterized by slowly progressing muscle weakness without cardiac or respiratory involvement [10]. Muscle computed tomography (CT) and MRI studies clearly show a relatively diffuse involvement in lower-leg muscles, while a selective pattern appears in thigh muscles [10,15,16]. Subtle mental impairment or peripheral nerve involvement was described in a previous report [17]. Mutations in the PH domain lead to an intermediate phenotype with mild respiratory failure and relatively severe weakness as compared to DNM2-CNM caused by middle-domain mutations [6]. Another study reported a more severe infantile form with hypotonia, weak suckling, and respiratory failure due to mutation in the PH domain of *DNM2* [11]. Although no *DNM2* mutations have

* Corresponding author. Tel.: +81 423461712; fax: +81 423461742.
E-mail address: nishino@ncnp.go.jp (I. Nishino).

0303-8467/$ – see front matter © 2011 Elsevier B.V. All rights reserved.
doi:10.1016/j.clineuro.2011.10.040

been identified among Japanese patients, there have been reports of patients with evidently similar clinicopathological features [4,5], suggesting the possibility of the presence of DNM2-CNM in the Japanese population. We therefore aimed at detecting *DNM2* mutations among Japanese CNM patients.

2. Materials and methods

2.1. Patients

We retrospectively recruited patients who were diagnosed with CNM or myotubular myopathy at the National Center of Neurology and Psychiatry and analyzed their samples from a total of 9639 muscle biopsies obtained between 1978 and 2006. Inclusion criteria were the presence of more than 6% centrally nucleated fibers and the absence of characteristic findings indicating other muscle diseases upon muscle biopsy. Our cohort consists of 22 unrelated patients aged 1–72 years: 2 had an AD family history; 5 had affected siblings, and consanguinity was documented in one of the patient's families; and 8 were sporadic cases. No record of family history was available for 7 patients. Direct sequence analysis previously performed on these patients excluded CTG expansion in the *DMPK* gene and *MTM1* mutations. Their clinical history was carefully reviewed. Additional medical information from affected family members was obtained by the attending neurologist, when possible.

2.2. Sequence analysis of DNM2

'All 22 patients and 4 members of 1 family were examined for *DNM2* sequence variants. DNA was extracted from blood or muscle samples using standard protocols. We sequenced all the exons and the exon–intron boundaries of *DNM2*. Both strands of PCR products were sequenced directly using BigDye Terminator v1.1 Sequencing Standard Kit (Applied Biosystems) with an automated ABI 3100 DNA sequencer with custom-made primers (Supplementary Table).

3. Results

3.1. Genetic diagnosis

Among 22 patients, we identified 3 mutations in 4 probands: c.1102G>A (p.E368K), c.1105C>T (p.R369W), and c.1393C>T (p.R465W), all of which were previously reported [6]. We further confirmed the mutations in affected family members of 2 patients (Table 1). We did not identify mutations from the families with consanguinity.

3.2. Clinical features

The clinicopathological features of patients with *DNM2* mutations are shown in Table 1. Clinical information for Patient 1-1 was not available. He was autopsied at the age of 17 years, at which point the gastrocnemius muscle was taken as a sample for analysis (Fig. 1A). The inheritance pattern was compatible with AD transmission in families 2 and 3, while it was sporadic in Patient 4-1.

Patients 2-1 and 3-2 were previously reported to have AD CNM or myotubular myopathy (Fig. 2A) [4,5]. In brief, Patient 2-1 noticed an ankle contracture at the age of 10 years and started having difficulty in climbing stairs at the age of 30 years. Achilles tendon elongation was performed at the age of 37 years, during which this patient was found to have atrophy of facial and distal muscles, and diminished tendon reflexes. He had mild ptosis, but ophthalmoplegia was not observed. Creatine kinase (CK) levels were within the normal range. nEMG was myogenic. Muscle biopsy of the rectus femoris at the age of 42 years showed 68% centrally nucleated fibers and a scattered radial distribution (Fig. 1B). CT of the patient's hamstring, soleus, and gastrocnemius muscles showed atrophy and fatty changes. There was no cardiac or respiratory involvement. Nerve conduction velocities were normal except for low-median compound action potentials that could be explained by muscle atrophy. Patient 2-2 exhibited ankle contracture, *pes cavus* due to plantaris muscle atrophy, and distal atrophy since 10 years of age and also underwent Achilles tendon elongation for ankle contracture in his second decade. No ptosis or ophthalmoplegia was observed.

Patient 3-2 noticed progressive lower-leg weakness, atrophy, and ankle contracture when he was 15 years old and he underwent achillotenotomy at 18 years of age. He developed dyspnea at the age of 54 years that necessitated a tracheotomy at the age of 55 years. Neurological findings at the age of 55 years revealed mild ptosis, distal muscle atrophy and weakness, and mild facial muscle involvement including ptosis. CK level was 48 IU/L. nEMG was myogenic. Sural nerve biopsy was unremarkable. Muscle biopsy of the peroneus brevis showed centrally placed nuclei in 40% of the fibers (Fig. 1C). The patient unfortunately died at the age of 58 years, and the primary cause of death was undetermined. His children (Patients 3-6, 3-7, 3-8, and 3-9 (Fig. 2B)) were found to have *pes cavus* caused by plantar muscle atrophy and were slow runners in their childhood.

At the age of 20 years, Patient 3-6 could not appose his palms when his wrists were extended and at the age of 35 years, he had difficulty in walking. He developed bilateral ankle contracture, because of which he had to stand and walk tiptoed. When he was 50 years old, neurological examination showed distal muscle weakness and atrophy with ankle- and finger-joint contractures (Fig. 3A–D). His deep tendon reflexes were also diminished. He lost his left eye in an accident during his childhood, but neither ophthalmoplegia in his right eye nor ptosis was observed. No peripheral nerve involvement was found on normal nerve conduction study. nEMG was myogenic. Results of echocardiography, Holter ECG, and pulmonary function tests were normal. Muscle biopsy of the biceps brachii at the age of 50 years was compatible with the CNM diagnosis (Fig. 1D–G).

The daughters of Patient 3-6 (Patients 3-10 and 3-11) followed a similar clinical course. They did not have ophthalmoplegia nor ptosis (Fig. 3G). Muscle CT showed marked atrophy in the posterior compartment of the lower extremities (gluteus maximus, hamstrings, gastrocnemius, and soleus) and thigh abductors, while only moderate atrophy and fatty changes were observed in the paraspinal muscles (Fig. 3E). Patient 3-11 had muscle involvement limited to the biceps femoris, gastrocnemius, and soleus as shown on CT at the age of 19 years (Fig. 3F). Both Patients 3-10 and 3-11 showed myogenic changes on nEMG, and the findings of nerve conduction studies were normal.

Patient 4-1 had no obvious family history (Fig. 3C). He noticed ankle contracture at the age of 30 and had gait disturbance at the age of 40 years. He underwent muscle biopsy at the age of 55 years. He was ambulant but did not use a cane. nEMG was actively myogenic, and the results of nerve conduction studies were normal.

In all patients, *pes cavus* caused by plantar muscle atrophy was the earliest sign that appeared before the age of 10 years. Atrophy of calf and posterior thigh muscles was seen during the second decade, but could be detected by muscle CT even in early stages (Fig. 3E and F). The clinical course was relatively benign, except for that of 1 patient who died at the age of 16 years (Patient 1-1), although no detailed information on the cause of death was available. Neither cardiac nor respiratory failure occurred in any patient, except Patient 3-2 who underwent tracheotomy for dyspnea secondary to severe pneumonia. All the 3 patients who were above 50 years of age are still ambulant. With an exception of Patient 3-2,

Table 1
Clinicopathological features of DNM2-CNM.

	Family		1	2			3			4
Demographic data	Patient number		1-1	2-1	3-2	3-6	3-7	3-10	3-11	4-1
	Mutation		c.1102G>A (p.E368K)	c.1393C>T (p.R465W)	c.1105C>T (p.R369W)	c.1105C>T (p.R369W)	c.1105C>T (p.R369W)	c.1105C>T (p.R369W)	c.1105C>T (p.R369W)	c.1105C>T (p.R369W)
	Age/sex		16/M	42/M	55/M	50/M	47/F	22/F	19/F	55/M
Clinical features	Ability to walk		NR	Ambulatory	With cane	With cane	Ambulatory	Ambulatory	Ambulatory	Ambulatory
	Opthalmoplegia		NR	–	–	–	–	–	–	–
	Ptosis		NR	+	+	–	–	–	–	–
	MMT upper extremities	Proximal	NR	5	5	5	4	4	4	4
		Distal	NR	5	5	2	3	2	2	3
	MMT lower extremities	Proximal	NR	4	5	4	3	3	4	4
		Distal	NR	4	5	2	2	2	2	3
	Deep tendon reflexes		NR	–	NR	N	↓	–	NR	↓
	Joint contractures		NR	Elbow, wrist, ankle	Ankle	Finger, wrist, elbow, spine, ankle	Finger, wrist, elbow, spine, ankle	Finger, wrist, elbow, spine, ankle	Finger, wrist, elbow, spine, ankle	Ankle
	Muscle atrophy	Leg	NR	+	+	+	+	+	+	+
		Paraspinal	NR	NR	NR	+	+	+	+	+
		Plantar	NR	+	+	+	+	+	+	+
	Cardiovascular		NR	N	N	NR	NR	N	N	N
	Respiratory		NR	NR	Tracheotomy	Normal vital capacity	Normal vital capacity	Normal vital capacity	Normal vital capacity	NR
Findings on muscle biopsy	Electromyography		NR	M	M	M	M	M	NT	M
	Nerve conduction studies		NR	*	N	N	N	N	N	NR
	Serum CK		NR	N	N	N	N	NR	N	N
	Muscle CT	Calf	NR	+	+	+	NR	NR	–	+
		Thigh	NR	2+	2+	2+	NR	NR	+	2+
	% of centrally nucleated fibers		65	68	55	60				70
	Radial distribution of myofibrils		+	+	NT	+				+
	Type 1 predominance (%)		80	79	NT	88				90
	Type 1 atrophy		+	+	NT	+				+
	Type 2B deficiency		+	+	NT	+				+
	Type 2C fibers (%)		2	1	NT	2				5

Abbreviations: MMT, manual muscle testing; +, present; –, absent; N, normal; NR, no record; NT, not tested; ↓, decreased; EMG, electromyography; M, myogenic changes; and NCS, nerve conduction study. The CT scores are as follows: 1+: decreased signal density and 2+: decreased signal density with severe muscle atrophy.

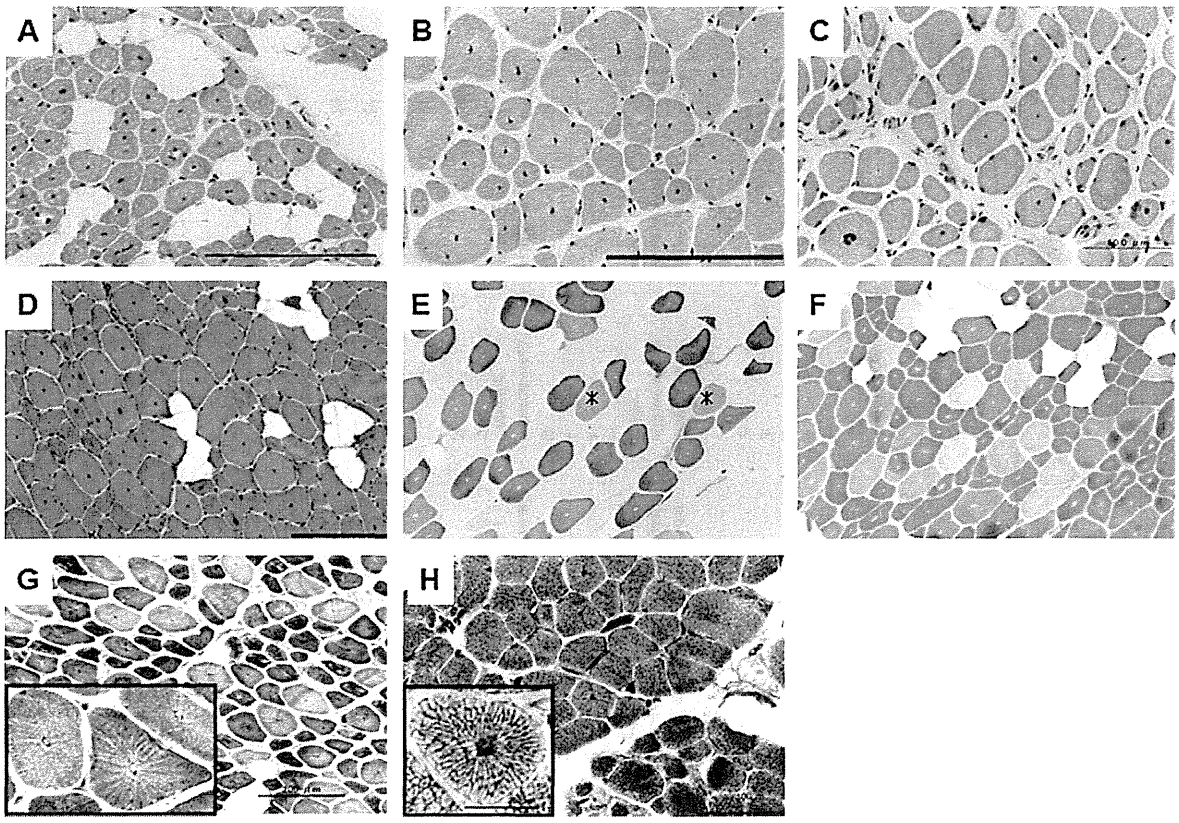

Fig. 1. Biopsy findings of DNM2-CNM (A-G) and non-DNM2-CNM (H). Hematoxylin and eosin stain of muscle sections from Patients 1-1 (A), 2-1 (B), 3-2 (C), and 3-6 (D). Numerous centronuclear fibers (up to 55%) and interstitial fibrosis were observed. Histochemical findings in muscle sections from Patient 3-6 (E–G). Type 1 predominance and hypotrophy (E, ATPase staining pH 10.6), a few type 2C fibers (F, ATPase pH 4.6), and radial distributions (G, NADH-TR) were observed. Radial distributions were also observed in some non-DNM2-CNM muscles (H, NADH-RT).

neither ptosis nor ophthalmoplegia was observed in the affected family members.

Clinical features of the CNM patients without *DNM2* mutations (non-DNM2-CNM) along with the number of patients are given below: proximal weakness (2/18), floppy infant (8/18), scoliosis (1/18), mental retardation (1/18), dysphagia (1/18), myalgia (1/18), and high-arched palate (8/10). Furthermore, only 1 of 10 patients with non-DNM2-CNM showed joint contracture. The clinical features of non-DNM2-CNM varied more widely than those of DNM2-CNM.

3.3. Summary of the pathological features

In all patients with DNM2-CNM, the pathological findings were rather similar: (1) radial distribution of myofibrils in scattered fibers, (2) type 1 fiber atrophy, (3) type 1 fiber predominance, and (4) a small number of type 2C fibers (Table 1, Fig. 1). In addition, the frequency with which muscle fibers with centrally placed nuclei were observed in DNM2-CNM patients was 63.1 ± 6.1% (mean ± SD), range, 55–70%, which is much lower than that observed in non-DNM2-CNM patients (24.7 ± 13.2%, range, 8–50%).

In contrast, none of the non-DNM2-CNM patients had all the 4 abovementioned pathological features. Definite radial distribution of myofibrils was seen only in 2 of 18 cases. In 4 of 18 cases, equivocal radial distribution was observed. Among the 18 cases, type 1 fiber atrophy was noted in 12 patients; type 1 fiber predominance, in 16 patients; and type 2C fibers, in 12 patients. In addition, type 2 fiber atrophy was seen in 2 of 18 patients.

4. Discussion

This is the first report to document *DNM2* mutations in CNM patients in Japan with a low frequency, similar to the cases found in Europe, the United States, Central Africa, and Argentina [7,10,11]. All affected family members had distal muscle atrophy, finger and ankle contractures, and *pes cavus* caused by plantar muscle atrophy in their childhood (Table 1, Fig. 3A–D). Atrophy and fatty changes in the gastrocnemius muscle were the earliest signs observed on CT and were noted in the second decade of their lives (Fig. 3E). Thigh flexor, gluteus maximus, and paraspinal muscles were involved in the later stages (Fig. 3F).

The clinical and pathological features of DNM2-CNM were rather homogeneous in our series, as in previous reports [6,10,16]. This can be helpful in establishing a working diagnosis in CNM patients. The phenotypes of the mutations identified here (E368K, R465W) were almost identical to those identified in previous cases [7], although only 1 patient with E368K and 1 with R369W showed ptosis and ophthalmoplegia. In addition, the early death of Patient 1-1 and the respiratory failure of Patient 3-2 are unusual occurrences for DNM2-CNM, although we could not obtain detailed information.

A high occurrence of ptosis (9/10 [10], 7/11 [18]) and ophthalmoplegia (2/10 [10], 5/11 [18]) among DNM2-CNM patients is observed in other countries [10], while in our series, ptosis was much more rare (2/8), and ophthalmoplegia was not seen in our

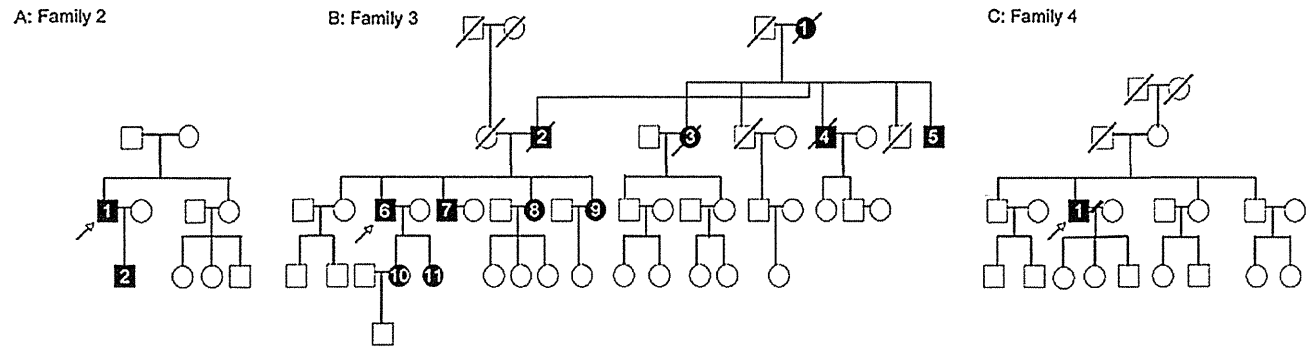

Fig. 2. The DNM2-CNM family tree. Families 2 and 3 had obvious autosomal dominant inheritance. On the contrary, Patient 4-1 had a sporadic onset. His parents and children did not show any symptoms.

cohort. In previous studies, most patients who did not have ptosis and ophthalmoplegia were from a p.R522H family, and most of them were infants [17]. The Japanese patients in our study, including those with the p.R465W mutation that causes DNM2-CNM with ptosis and ophthalmoplegia, as shown in a European study, did not have ophthalmoplegia, and only 2 (p.R465W and R369W) patients exhibited ptosis. Ethnic background may be a contributing factor to the occurrence of ptosis because there are some anatomical differences between the eyelids of Asian and European populations: Asians have shallower eyelids than Europeans [18,19]. Since the severity of ptosis is correlated to the severity of myopathy, ptosis caused by mutations in the middle domain in *DNM2* in DNM2-CNM patients could be mild enough not to be recognized in the eyelids of Asians.

On the other hand, among non-DNM2-CNM patients, ptosis or ophthalmoplegia was also seen in 4 of 18 cases, suggesting that ocular symptoms may not be a specific indicator of *DNM2* mutations

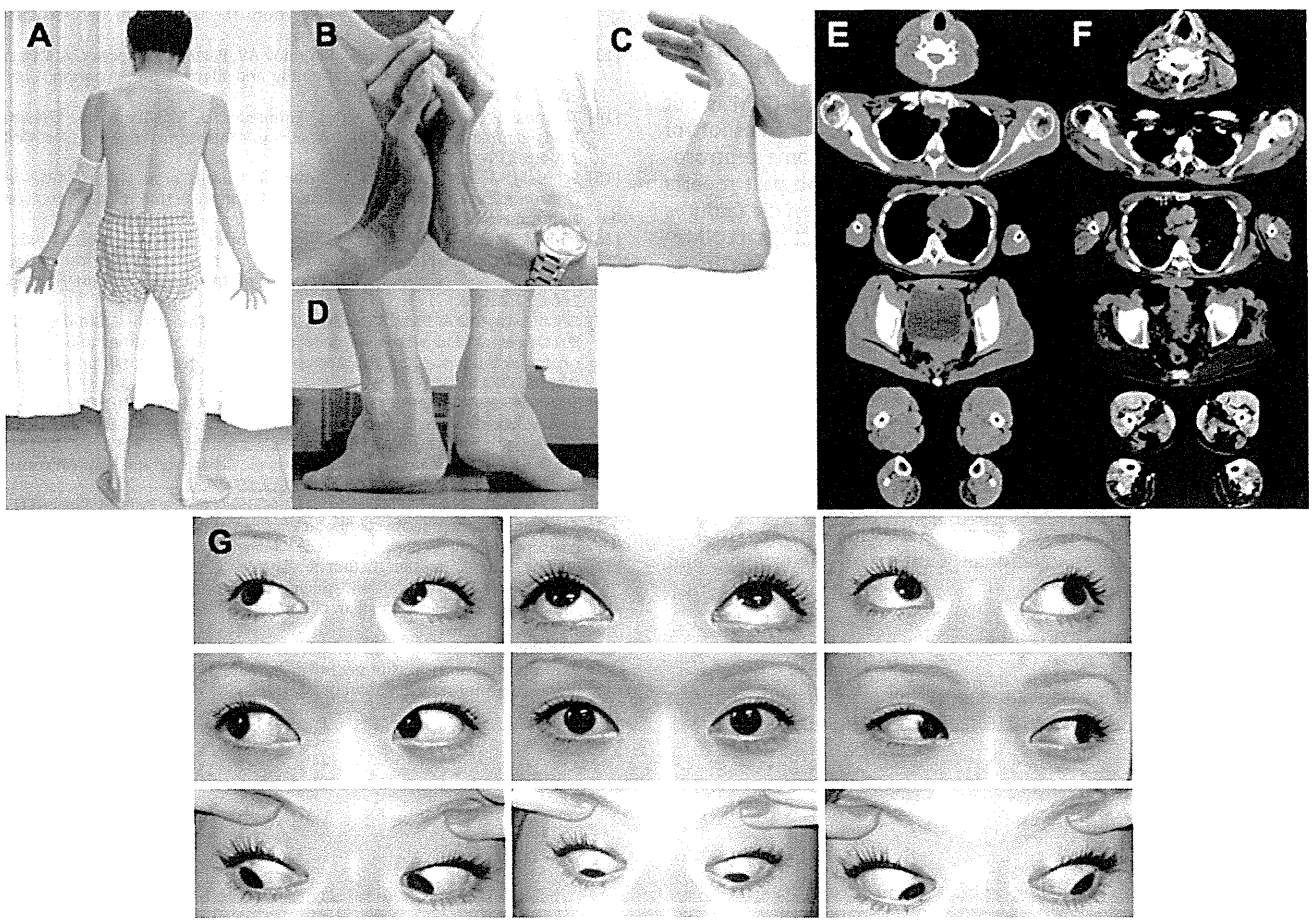

Fig. 3. Photograph of Patient 3-6: distal muscular atrophy (A), joint contracture of fingers (B), and ankle contracture (C); patient could not put his heels on the floor because of the ankle contracture (D). Muscle CT of Patient 3-6 (F) and Patient 3-11 (E) depicting lower-leg muscle atrophy of the posterior compartment (gluteus maximus, hamstrings, gastrocnemius, and soleus), thigh abductor, and paraspinal muscles. Note the early involvement of the biceps femoris, gastrocnemius, and soleus in Patient 3-11 when she was 19 years old. Ophthalmoplegia and ptosis are not observed in most patients (G: Patient 3-11).

in CNM patients, at least in Japanese patients, further highlighting the importance of the frequency of ocular involvement as a genetic factor.

Other symptoms of the central nervous system and peripheral neuropathy were also observed in our cohort and were reported as subtle complications of DNM2-CNM [17]. Among the non-DNM2-CNM patients, other causative genes for CNM were considered. *MTM1* mutations are implicated in CNM, but in our cohort, *MTM1* mutations were excluded. Compound heterozygous mutations in *hJUMPY*, a gene that encodes a phosphoinositide phosphatase, were reported as a cause of sporadic CNM [8]. Additionally, *BIN1* is a newly identified causative gene for autosomal recessive CNM [9]; patients with autosomal recessive CNM show typical CNM muscle pathology and proximal-dominant muscle weakness, which is more severe than observed in DNM2-CNM patients. The pathology of CNM with *BIN1* mutations does not have a radial distribution, which is thought to be a hallmark of DNM2-CNM [9]. Notably, some of our non-DNM2-CNM patients showed a radial distribution. However, none of our non-DNM2-CNM patients had a family history that would indicate autosomal recessive inheritance and merit further mutational analysis of the *hJUMPY* and *BIN1* genes. Other candidate genes include *Srpk3* [20] and *PTPLA* [21], which were thus far implicated as causative genes of CNM in mice and dogs.

DNM2 mutations were also identified in AD Charcot–Marie–Tooth disease (CMT) [22]; in fact, some DNM2-CNM patients also show very mild reductions in nerve conduction velocities in the lower legs [10] or pathological changes in both myelinated and unmyelinated nerve fibers [18]. Nevertheless, none of our patients showed any abnormality in nerve conduction studies, suggesting that peripheral nerve involvement does not occur frequently in DNM2-CNM patients.

Although the precise pathomechanism of DNM2-CNM is not known, mutations are thought to hinder either the transport of DNM2 to the centrosome or its interaction with some centrosomal component [7]. Interestingly, in our study and past reports of *DNM2* mutations in the middle domain, characteristic features were observed in muscle pathology, as opposed to neonatal DNM2-CNM with PH domain mutations in which centrally nucleated fibers and radial distribution of myofibers are less prominent [11].

Acknowledgements

This work was supported in part by Research on Intractable Diseases of Health and Labour Sciences Research Grants, Comprehensive Research on Disability Health and Welfare, Health and Labour Science Research Grants, Intramural Research Grant (23-5 23-4) for Neurological and Psychiatric Disorders of NCNP and Young Investigator Fellowship from Translational Medical Center, National Center of Neurology and Psychiatry.

Appendix A. Supplementary data

Supplementary data associated with this article can be found, in the online version, at doi:10.1016/j.clineuro.2011.10.040.

References

[1] North K. In: Engel AG, Franzini-Armstrong C, Myology, editors. Congenital myopathies. 3rd ed. New York: McGraw-Hill; 2004. p. 1494–5.
[2] Jeannet PY, Mittaz L, Dunand M, Laforêt P, Urtizberea JA, Rouche A, et al. Clinical and histologic findings in autosomal centronuclear myopathy. Neurology 2004;11:1484–90.
[3] Wallgren-Petterson C, Clarke A, Samson F, Fardeau M, Dubowitz V, Moser H, et al. The myotubular myopathies: differential diagnosis of the X linked recessive, autosomal dominant, and autosomal recessive forms and present state of DNA studies. J Med Genet 1995;32:673–9.
[4] Sakuma T, Nakajima H, Fujimura C, Kimura F, Hanabusa T. A case of centronuclear myopathy with Charcot–Marie–Tooth disease-like lower leg muscle atrophy. Naika 2004;54:192–4 [in Japanese].
[5] Wakabayashi Y, Arimura Y, Sawaguchi Y, Koike F, Yoshino K. A case of myotubular myopathy with autosomal dominant inheritance. No to Shinkei 1980;32:715–22 [in Japanese].
[6] Bitoun M, Bevilacqua JA, Eymard B, Prudhon B, Fardeau M, Guicheney P, et al. A new centronuclear myopathy phenotype due to a novel dynamin 2 mutation. Neurology 2009;6:93–5.
[7] Bitoun M, Maugenre S, Jeannet PY, Lacène E, Ferrer X, Laforêt P, et al. Mutations in dynamin 2 cause dominant centronuclear myopathy. Nat Genet 2005;37:1207–9.
[8] Tosch V, Rohde HM, Tronchère H, Zanoteli E, Monroy N, Kretz C, et al. A novel PtdIns3P and PtdIns (3,5) P_2 phosphatase with an inactivating variant in centronuclear myopathy. Hum Mol Genet 2006;1:3098–106.
[9] Nicot AS, Toussaint A, Tosch V, Zanoteli E, Monroy N, Kretz C, et al. Mutations in *amphiphysin 2* (*BIN1*) disrupt interaction with dynamin 2 and cause autosomal recessive centronuclear myopathy. Nat Genet 2007;39:1134–9.
[10] Fischer D, Herasse M, Bitoun M, Barragán-Campos HM, Chiras J, Laforêt P, et al. Characterization of the muscle involvement in dynamin 2-related centronuclear myopathy. Brain 2006;129:1463–9.
[11] Bitoun M, Bevilacqua JA, Prudhon B, Barragán-Campos HM, Chiras J, Laforêt P, et al. Dynamin 2 mutations cause sporadic centronuclear myopathy with neonatal onset. Ann Neurol 2007;6:666–70.
[12] Jones SM, Howell KE, Henley JR, Cao H, McNiven MA. Role of dynamin in the formation of transport vesicles from the trans-Golgi network. Science 1998;23:573–7.
[13] Schafer DA, Weed SA, Binns D, Karginov AV, Parsons JT, Cooper JA. Dynamin2 and cortactin regulate actin assembly and filament organization. Curr Biol 2002;29:1852–7.
[14] Thompson HM, Cao H, Chen J, Euteneuer U, McNiven MA. Dynamin 2 binds gamma-tubulin and participates in centrosome cohesion. Nat Cell Biol 2004;6:335–42.
[15] Schessl J, Medne L, Hu Y, Zou Y, Brown MJ, Huse JT, et al. MRI in *DNM2*-related centronuclear myopathy: evidence for highly selective muscle involvement. Neuromuscul Disord 2007;17:28–32.
[16] Jeub M, Bitoun M, Guicheney P, Kappes-Horn K, Strach K, Druschky KF, et al. Dynamin 2-related centronuclear myopathy: clinical, histological and genetic aspects of further patients and review of the literature. Clin Neuropathol 2008;27:430–8.
[17] Echaniz-Laguna A, Nicot AS, Carrê S, Franques J, Tranchant C, Dondaine N, et al. Subtle central and peripheral nervous system abnormalities in a family with centronuclear myopathy and a novel dynamin 2 gene mutation. Neuromuscul Disord 2007;17:955–9.
[18] Susman RD, Quijano-Roy S, Yang N, Webster R, Clarke NF, Dowling J, et al. Expanding the clinical, pathological and MRI phenotype of *DNM2*-related centronuclear myopathy. Neuromuscul Disord 2010;20:229–37.
[19] Liu D, Hsu WM. Oriental eyelids. Anatomic difference and surgical consideration. Ophthal Plast Reconstr Surg 1986;2:59–64.
[20] Nakagawa O, Arnold M, Nakagawa M, Hamada H, Shelton JM, Kusano H, et al. Centronuclear myopathy in mice lacking a novel muscle-specific protein kinase transcriptionally regulated by MEF2. Genes Dev 2005;19:2066–77.
[21] Pele M, Tiret L, Kessler JL, Blot S, Panthier JJ. SINE exonic insertion in the PTPLA gene leads to multiple splicing defects and segregates with the autosomal recessive centronuclear myopathy in dogs. Hum Mol Genet 2005;1: 1417–27.
[22] Züchner S, Noureddine M, Kennerson M, Verhoeven K, Claeys K, De Jonghe P, et al. Mutations in the pleckstrin homology domain of dynamin 2 cause dominant intermediate Charcot–Marie–Tooth disease. Nat Genet 2005;37: 289–94.

The American Journal of Pathology, Vol. 180, No. 4, April 2012

DOI: 10.1016/j.ajpath.2011.12.040

Molecular Pathogenesis of Genetic and Inherited Diseases

In Vivo Characterization of Mutant Myotilins

Etsuko Keduka,* Yukiko K. Hayashi,* Sherine Shalaby,* Hiroaki Mitsuhashi,*† Satoru Noguchi,* Ikuya Nonaka,* and Ichizo Nishino*

From the Department of Neuromuscular Research, National Institute of Neuroscience, National Center of Neurology and Psychiatry, Tokyo, Japan; and the Division of Genetics,† Children's Hospital Boston, Harvard Medical School, Boston, Massachusetts*

Myofibrillar myopathy (MFM) is a group of disorders that are pathologically defined by the disorganization of the myofibrillar alignment associated with the intracellular accumulation of Z-disk–associated proteins. MFM is caused by mutations in genes encoding Z-disk–associated proteins, including myotilin. Although a number of MFM mutations have been identified, it has been difficult to elucidate the precise roles of the mutant proteins. Here, we present a useful method for the characterization of mutant proteins associated with MFM. Expression of mutant myotilins in mouse tibialis anterior muscle by *in vivo* electroporation recapitulated both the pathological changes and the biochemical characteristics observed in patients with myotilinopathy. In mutant myotilin-expressing muscle fibers, myotilin aggregates and is costained with polyubiquitin, and Z-disk–associated proteins and myofibrillar disorganization were commonly seen. In addition, the expressed S60C mutant myotilin protein displayed marked detergent insolubility in electroporated mouse muscle, similar to that observed in human MFM muscle with the same mutation. Thus, *in vivo* electroporation can be a useful method for evaluating the pathogenicity of mutations identified in MFM. ***(Am J Pathol 2012, 180: 1570–1580; DOI: 10.1016/j.ajpath.2011.12.040)***

Myofibrillar myopathy (MFM) is a group of neuromuscular diseases with common morphological features such as disorganized myofibrillar alignment and accumulation of Z-disk–associated proteins.[1] Mutations in genes encoding Z-disk–associated proteins are known to cause MFM. Disease-associated mutations have been identified in six genes, including myotilin, desmin, αB-crystallin, ZASP, filamin C, and BAG3.[2,3] Elucidation of their pathogenicity, however, is sometimes difficult.

Myotilin (myofibrillar protein with titin-like immunoglobulin domains) is a 57-kDa protein with 10 exons encoded by the myotilin gene (*MYOT*) on chromosome 5q31. Myotilin consists of a unique serine-rich domain at the N-terminus and two Ig-like domains at the C-terminus.[4–7] Myotilin is highly expressed in skeletal and cardiac muscle, and localizes to the Z-disk,[4] which plays important roles in sarcomere assembly, actin filament stabilization, and muscle force transmission.[8,9] Myotilin interacts with several Z-disk–associated proteins, including α-actinin,[4] filamin C,[10,11] FATZ,[11] ZASP,[12] and MuRF ubiquitin ligase.[13] Myotilin also interacts with actin monomers and filaments through its Ig-like domains, which also mediate homodimerization.[14] Previous studies have shown that myotilin can bundle actin filaments *in vitro*, acting alone or in collaboration with α-actinin and filamin C.[4,14,15] Thus, myotilin is thought to play a role in anchoring and stabilizing actin filaments at the Z-disk, and is involved in the organization and maintenance of Z-disk integrity.[12] Missense mutations in *MYOT* have been associated with MFM,[16–18] limb girdle muscular dystrophy type 1A,[17,19,20] and distal myopathy.[21,22] We have previously identified a mutation p.Arg405Lys (R405K) in exon 9 in the second Ig-like domain of myotilin. The R405K mutant myotilin exhibited defective homodimerization and decreased interaction with α-actinin in a yeast 2-hybrid (Y2H) system.[23] All of the other previously reported *MYOT* mutations are located in exon 2 [14,16–18,24], with p.Ser60Cys (S60C) being one of the most common mutations. The pathogenic effects of *MYOT* mutations and

Supported by a Grant-in-Aid for Scientific Research from the Japan Society for the Promotion of Science; a Comprehensive Research on Disability Health and Welfare (20B-12, 20B-13) award from the Ministry of Health, Labor and Welfare; a Research on Intractable Diseases award from the Ministry of Health, Labor and Welfare; an Intramural Research Grant (23-4, 23-5, 23-6) for Neurological and Psychiatric Disorders, National Center of Neurology and Psychiatry; and a grant from the Japan Foundation for Neuroscience and Mental Health.

Accepted for publication December 29, 2011.

Supplemental material for this article can be found at *http://ajp.amjpathol.org* or at doi: 10.1016/j.ajpath.2011.12.040.

Address reprint requests to Yukiko K. Hayashi, M.D, Ph.D., Department of Neuromuscular Research, National Institute of Neuroscience, National Center of Neurology and Psychiatry, 4-1-1 Ogawahigashicho, Kodaira, Tokyo, 187-8502, Japan. E-mail: hayasi_y@ncnp.go.jp.

the disease mechanism involved remain poorly understood.

Model animals, such as transgenic mice, have contributed to understanding of the critical pathogenic events in MFM.[25-27] Some MFMs, including myotilinopathies, are late-onset and slowly progressive diseases.[1,3] To reproduce clinical and pathological features in model animals for such late-onset mild myopathy is both labor intensive and time consuming. Among the 10 missense mutations identified to date in patients with myotilinopathy,[14,16-18,23,24] only the Thr57Ile (T57I) mutation reproduces the pathological changes in transgenic mice after 12 months of age.[28] To screen for candidate mutations in MFM, a new method is required for demonstrating the pathogenicity of mutations. In the present study, we expressed mutant myotilin in mouse muscle by *in vivo* electroporation and were able to easily reproduce pathological changes similar to those observed in skeletal muscle from patients with *MYOT* mutations.

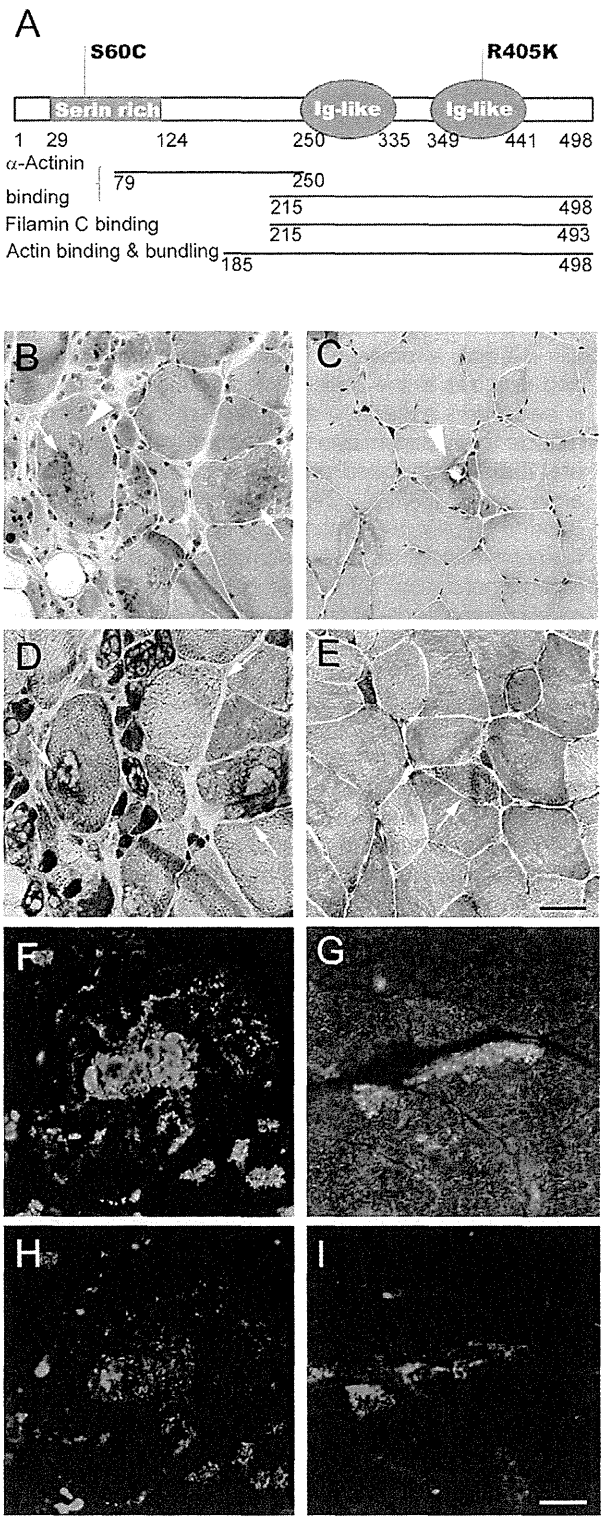

Materials and Methods

Clinical Materials

All clinical materials used in this study were obtained for diagnostic purposes with written informed consent. The studies were approved by the Ethical Committee of the National Center of Neurology and Psychiatry.

Genetic Analysis

Genomic DNA was isolated from peripheral lymphocytes or muscle specimens of patients, using standard techniques. Sequencing and mutation analysis of *MYOT* were performed as described previously.[23]

Plasmid Construction

We cloned full-length human myotilin cDNA and generated mutant myotilin (mMYOT) by site-directed mutagenesis, as described previously.[23] A C→G substitution at nucleotide position 179 and a G→A substitution at nucleotide 1214 were introduced to obtain p.S60C and p.R405K, respectively. A schematic of the location of these mutations in the structure of the myotilin protein is given in Figure 1A. For expression in mammalian cells, cDNAs of wild-type myotilin (wtMYOT) or mMYOT (S60C or R405K) were subcloned into pCMV-Myc vector (Ta-

Figure 1. Myotilin mutations and histopathological findings in myotilinopathy patients. **A:** Myotilin structure and disease-related mutations. p.Ser60Cys (S60C) is located in the serine-rich domain and p.Arg405Lys (R405K) is located in the second immunoglobulin (Ig)-like domain of myotilin. **B–I:** Pathological changes in muscles from patient 1 with *MYOT*S60C (**B**, **D**, **F**, and **H**) and from patient 2 with *MYOT*R405K (**C**, **E**, **G**, and **I**). **B:** Modified Gömöri trichrome (mGT) staining of biopsied skeletal muscle from patient 1 revealed markedly degenerated fibers with many spheroid protein inclusions (**arrows**). Some fibers had rimmed vacuoles (**arrowhead**). **C:** mGT staining of biopsied skeletal muscle from patient 2 revealed scattered fibers with rimmed vacuoles (**arrowhead**). **D:** NADH tetrazolium reductase (NADH-TR) staining of the serial section shown in **B** revealed markedly disorganized intermyofibrillar networks (**arrows**). **E:** NADH-TR staining of the serial section shown in **C** revealed disorganized intermyofibrillar networks (**arrow**). **F–I:** Coimmunostaining of muscles from patients using anti-myotilin (green) and anti-polyubiquitin (red) antibodies. **F:** Large accumulations of myotilin were observed in many fibers in patient 1. **G:** Small accumulations of myotilin were seen in some fibers in patient 2. Myotilin aggregates were positive for polyubiquitin in both patient 1 (**H**) and patient 2 (**I**). Scale bars: 50 μm (**B–E**); 20 μm (**F–I**).

kara Bio, Shiga, Japan). All constructs were verified by sequencing. Primer sequences are available on request.

Cell Culture, Transfection, and Immunocytochemical Analysis

C2C12 murine myoblast cells (American Type Culture Collection, Manassas, VA) were cultured in Dulbecco's modified Eagle's medium (Sigma-Aldrich, St. Louis, MO) supplemented with 10% fetal bovine serum (Invitrogen, Carlsbad, CA) at 37°C in a humidified atmosphere of 5% carbon dioxide. The cells were transiently transfected using FuGENE HD transfection reagent (Roche Diagnostics, Indianapolis, IN), according to the manufacturer's instructions. Forty-eight hours after transfection, the cells were fixed in 4% paraformaldehyde, permeabilized with 0.5% Triton-X 100, and costained with anti-Myc antibody (Sigma-Aldrich) and rhodamine-labeled phalloidin (Wako Pure Chemical Industries, Osaka, Japan) to detect transfected myotilin and actin filaments, respectively, according to standard protocol.[29]

In Vivo *Electroporation*

ICR mice were purchased from CLEA Japan (Fuji, Shizuoka, Japan). Animals were handled in accordance with the guidelines established by the Ethical Review Committee on the Care and Use of Rodents in the National Institute of Neuroscience, National Center of Neurology and Psychiatry. All mouse experiments were approved by the Committee. Five-week-old male ICR mice were anesthetized with diethyl ether, and the tibialis anterior (TA) muscles of mice were injected with 80 μg of purified Myc-tagged myotilin plasmid DNA. wtMYOT was injected to one side of TA muscle and mMYOT (S60C or R405K) was injected to the other side of TA muscle. *In vivo* transfection was performed using a square-wave electroporator (CUY-21SC; Nepa Gene, Ichikawa, Japan). A pair of electrode needles was inserted into the muscle to a depth of 3 mm to encompass the DNA injection sites. Each injected site was administered with three consecutive 50 ms-long pulses at the required voltage (50 to 90 V) to yield a current of 150 mA. After a 1-second interval, three consecutive pulses of the opposite polarity were administered. At 7 or 14 days after electroporation, mice were sacrificed by cervical dislocation, and TA muscles were isolated.

Histochemical and Immunohistochemical Analyses

Biopsied human muscles or electroporated mouse TA muscles were frozen in isopentane cooled in liquid nitrogen. Serial 10-μm cryosections were stained with modified Gömöri trichrome (mGT) and NADH-tetrazolium reductase (NADH-TR) and were subjected to a battery of histochemical methods. Immunohistochemistry was performed on serial 6-μm cryosections, as described previously.[29]

Antibodies

The primary antibodies used in this study were as follows: actin (Kantoukagaku, Tokyo, Japan), α-actinin (Sigma-Aldrich), BAG3 (Abcam, Tokyo, Japan), αB-crystallin (StressGen Biotechnologies, Victoria, BC, Canada), desmin (PROGEN Biotechnik, Heidelberg, Germany), filamin C (kindly provided by A.H. Beggs),[30] c-Myc (Sigma-Aldrich), c-Myc (PROGEN Biotechnik), myotilin (Proteintech Group, Chicago, IL), polyubiquitinated protein (Biomol International-Enzo Life Sciences, Plymouth Meeting, PA), GAPDH (Advanced ImmunoChemical, Long Beach, CA), and horseradish peroxidase-labeled anti-c-Myc antibody (Santa Cruz Biotechnology, Santa Cruz, CA).

Evaluation of Aggregates

Histochemical and immunohistochemical analyses were performed on cryosections of electroporated muscles sectioned at 500-μm intervals. The section containing the highest number of Myc-positive fibers (>100 fibers) was used. Myc-positive granules >1 μm in diameter were defined as aggregates. The Myc-positive fibers containing Myc-positive aggregates were counted among all Myc-positive fibers. Five mice each from the wtMYOT-, mMYOT S60C-, and mMYOT R405K-expressing groups were examined. To compare the number and size of Myc-positive aggregates per fiber, we measured the number and area of Myc-positive aggregates in 30 myofibers from each specimen using ImageJ software version 1.43 (NIH, Bethesda, MD). The results are presented as bar graphs (±SD) and histograms. Fifteen serial sections were immunoblotted to measure the amounts of electroporated Myc-tagged myotilin protein.

Electron Microscopy

For electron microscopy, cryosections (25 μm thick) of biopsied muscle with the S60C mutation (patient 1) were fixed with 2% glutaraldehyde in 100 mmol/L cacodylate buffer for 15 minutes on ice. After a shaking with a mixture of 4% osmium tetroxide, 1.5% lanthanum nitrate, and 200 mmol/L s-collidine for 1 to 2 hours, samples were embedded in epoxy resin. TA muscles of 5-week-old ICR mice were coelectroporated with pEGFP-C1 plasmid (Clontech, Tokyo, Japan), which encodes enhanced green fluorescent protein (EGFP), and with either Myc-wtMYOT or Myc-mMYOT (S60C or R405K) plasmid (40 μg each). As a control, pEGFP-C1 plasmid was electroporated alone. TA muscles were isolated 7 and 14 days after electroporation. EGFP-positive regions were trimmed under a fluorescence microscope and fixed with 2% glutaraldehyde in 100 mmol/L cacodylate buffer for 3 hours. After a shaking with a mixture of 4% osmium tetroxide, 1.5% lanthanum nitrate, and 200 mmol/L s-collidine for 2 to 3 hours, samples were embedded in epoxy resin. Semithin sections (1 μm thick) were stained with Toluidine Blue. Ultrathin sections (100 nm thick) were stained with uranyl acetate and lead citrate, and were analyzed at 120 kV using a Tecnai Spirit transmission electron microscope (FEI, Hillsboro, OR).

Solubility and Immunoblot Assay

To examine solubility of mutant myotilin, we used frozen biopsied muscles from human control subjects and from the two myotilinopathy patients, as well as TA muscles of six mice each from the wtMYOT-, mMYOT S60C-, and mMYOT R405K-expressing groups, at 14 days after electroporation. The 1.25-mm^3 specimens of muscle were lysed and homogenized in 150 μL of radioimmunoprecipitation assay buffer containing 50 mmol/L Tris-HCl (pH 7.5), 150 mmol/L NaCl, 1 mmol/L EDTA (pH 8.0), 1% Nonidet P-40, 0.5% sodium deoxycholate, 0.1% SDS, and Roche complete protease inhibitor cocktail (Roche Diagnostics). The lysates were incubated at 4°C for 20 minutes with gentle rotation, and then centrifuged at 15,000 × *g* at 4°C for 20 minutes. The supernatants and precipitates were collected, and the protein concentrations of the supernatants were determined using a protein assay kit (Bio-Rad Laboratories, Hercules, CA). Immunoblotting of the supernatant (detergent-soluble) and precipitate (detergent-insoluble) fractions was performed, as described previously.[23] Glyceraldehyde 3-phosphate dehydrogenase (GAPDH) was used as an internal standard. Immunoreactive complexes on the membranes were detected using enhanced chemiluminescence ECL Plus detection reagent (GE Healthcare, Chalfont St Giles, UK). Insolubility index was calculated as the ratio of the quantity of insoluble protein to the total quantity of proteins (the sum of soluble and insoluble proteins).

Immunoprecipitation

The 5-mm^3 specimens of frozen electroporated mouse muscles isolated at 14 days after electroporation were lysed and homogenized in 0.6 mL of radioimmunoprecipitation assay buffer. The lysates were incubated at 4°C for 20 minutes with gentle rotation, and then centrifuged at 15,000 × *g* at 4°C for 20 minutes. The supernatants were collected, and their protein concentrations were adjusted using a protein assay kit (Bio-Rad Laboratories). Immunoprecipitation was performed as described previously,[23] with agarose-conjugated anti-Myc antibody (Santa Cruz Biotechnology).

Statistical Analysis

Differences between wtMYOT-, mMYOT S60C-, and mMYOT R405K-expressing mice were analyzed with GraphPad Prism version 5 (GraphPad Software, La Jolla, CA). Comparisons among groups were performed by one-way analysis of variance with post hoc Tukey's analysis. Data are expressed as means ± SD.

Results

Mutation Screening and Histochemical Analyses of Muscles from Patients

We performed *MYOT* mutation screening in MFM patients and identified two patients with mutations. Patient 1, harboring a *MYOT* c.179C→G (p.S60C) mutation in exon 2, was a 63-year-old woman with a 6-year-long history of slowly progressive limb muscle weakness. Her mother (deceased) had had muscle weakness. The patient had difficulty in climbing stairs without support, and could not walk for long distances. Her serum creatine kinase level was elevated to 734 IU/L (reference, <200 IU/L). A biopsied specimen from the rectus femoris muscle showed marked variation in fiber size, with some necrotic fibers. Clusters of degenerated fibers with abnormal cytoplasmic inclusions were observed; some fibers with rimmed vacuoles were also seen (Figure 1B). Intermyofibrillar networks were markedly disorganized (Figure 1D). Under electron microscopy, electron-dense materials and cytoplasmic amorphous inclusions of various sizes were seen in some fibers (see Supplemental Figure S1 at *http://ajp.amjpathol.org*). Patient 2 was a 57-year-old woman harboring a *MYOT* c.1214G→A (p.R405K) mutation in exon 9. Detailed clinical symptoms have been described previously.[23] In brief, this patient had a 16-year-long history of slowly progressive proximal limb muscle weakness. Her serum creatine kinase level was mildly elevated (385 IU/l). A specimen from the vastus lateralis muscle showed marked variation in fiber size, scattered fibers with internal nuclei, and small angular fibers. Some fibers with rimmed vacuoles were seen (Figure 1C), and intermyofibrillar networks were disorganized (Figure 1E). Immunohistochemical analysis of muscle specimens from both patients revealed scattered fibers with strong immunoreactive accumulations of myotilin (Figure 1, F and G), which costained with polyubiquitin (Figure 1, H and I), α-B crystallin, BAG3, actin, desmin, and filamin C (see Supplemental Figure S2 at *http://ajp.amjpathol.org*).

Mutant Myotilin Does Not Aggregate in Cultured Cells

To examine the aggregation of mutant myotilins in cultured cells, C2C12 murine myoblasts were transfected with Myc-tagged wtMYOT (Myc-wtMYOT) or Myc-tagged mMYOT (Myc-mMYOT S60C or R405K). After 48 hours, immunostaining with anti-Myc antibody and rhodamine-labeled phalloidin revealed that the expressed Myc-wtMYOT, Myc-mMYOT S60C, and Myc-mMYOT R405K did not form abnormal protein aggregations, and they localized at actin stress fibers (Figure 2). Expression of mMYOT did not affect differentiation of C2C12 cells (data not shown).

Accumulation of Myotilin after Electroporation

To investigate the roles of mutant myotilin, we performed *in vivo* electroporation to express Myc-wtMYOT or Myc-mMYOT (S60C or R405K) in mouse TA muscles. At 7 and 14 days after electroporation, Myc-positive granules with diameters >1 μm were observed in Myc-tagged myotilin-expressing myofibers (Figure 3A). Compared with wtMYOT-expressing myofibers, mMYOT-expressing myofi-

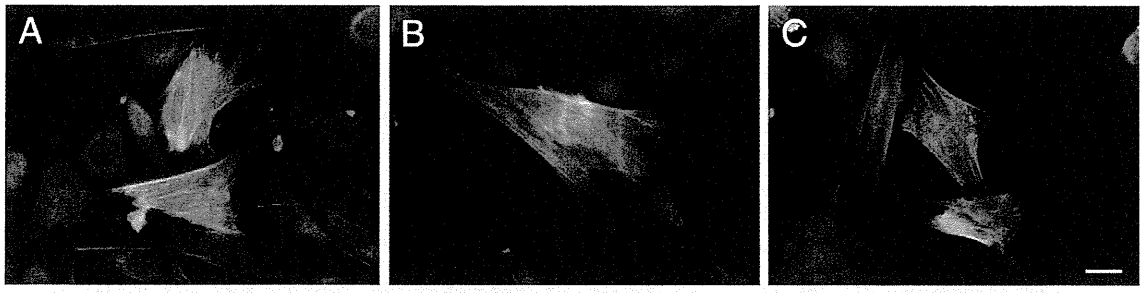

Figure 2. Expression of mutant myotilin in cultured cells. Immunofluorescence staining of transfected Myc-wtMYOT (**A**), Myc-mMYOT S60C (**B**), and Myc-mMYOT R405K (**C**) in C2C12 murine myoblasts. Merged images of Myc-tagged myotilin-expressing cells (green) costained for actin stress fibers (red), and nuclear staining with DAPI (blue). C2C12 myoblasts expressing mMYOT S60C (**B**) or R405K (**C**) did not exhibit protein aggregates, and the mutant myotilin colocalized with actin stress fibers similar to wtMYOT (**A**). Scale bar = 20 μm.

bers contained more granular aggregates that were larger in size. At 7 days after electroporation, Myc-positive aggregates of wtMYOT, mMYOT S60C, and mMYOT R405K were observed in 14 ± 5%, 44 ± 7%, and 21 ± 4% of muscle fibers, respectively (Figure 3B). At 14 days after electroporation, the number of the fibers with aggregates increased to 22 ± 4% in wtMYOT, 50 ± 2% in mMYOT S60C, and 37 ± 3% in mMYOT R405K (Figure 3C). The number and size of Myc-positive aggregates in 30 randomly selected Myc-positive muscle fibers were much higher in mMYOT S60C and slightly higher in mMYOT R405K at 14 days after electroporation than at 7 days (see Supplemental Figure S3 at *http://ajp.amjpathol.org*). These data indicate that the expressed mutant myotilins, and mMYOT S60C in particular, are prone to aggregate in skeletal muscles. The amounts of expressed Myc-tagged myotilin proteins were approximately equal, as measured by immunoblotting (Figure 3D).

Myofibril Disorganization and Z-Disk Streaming in Muscles Expressing Mutant Myotilins

To investigate the ultrastructural characteristics of mutant myotilin-electroporated muscles, we performed electron microscopy at 7 and 14 days after electroporation. In Toluidine Blue-stained longitudinal semithin sections, partial disorganization of the Z-disk was observed in both mMYOT S60C-expressing and mMYOT R405K-expressing TA muscles, but not in control or wtMYOT electroporated muscles (data not shown). Electron microscopy also revealed myofibril disorganization with disrupted Z-disk, such as Z-disk streaming and broadening, in mMYOT-expressing muscles (Figure 4, A and D). Variable-sized (1 to 8 μm in diameter) electron-dense material, with electron densities similar to that of the Z-disk, were also seen in mMYOT-expressing mouse muscles (Figure 4, B and E). The inclusions were occasionally associated with autophagic vacuoles (Figure 4, C and F). These ultrastructural findings were commonly observed in both mMYOT S60C- and mMYOT R405K-expressing mouse muscles.

Mutant Myotilin Aggregates Colocalize with Polyubiquitin and Other Z-Disk–Associated Proteins

To compare the protein accumulations in human and mouse muscles, we performed immunohistochemical analysis. At 14 days after electroporation, some cytoplasmic inclusions were observed in mGT-stained sections of mMYOT-expressing muscles (Figure 5, A and B). Immunostaining of serial sections revealed that the inclusions were immunopositive for the Myc tag (Figure 5, A and B). The aggregates of Myc-mMYOT (S60C and R405K) strongly colocalized with polyubiquitin and αB-crystallin. Accumulations of other Z-disk–associated proteins were also observed, including BAG3, actin, desmin, and filamin C (Figure 5). These findings are similar to the observations made in the patients' muscles (Figure 1, F–I; see also Supplemental Figure S2 at *http://ajp.amjpathol.org*). In the electroporated muscles, Myc-wtMYOT aggregates also colocalized with Z-disk–associated proteins, including αB-crystallin, BAG3, actin, desmin, and filamin C (data not shown), whereas only few wtMYOT aggregates were immunopositive for polyubiquitin (Figure 6A).

Mutant Myotilin Proteins Display Marked Detergent Insolubility with Polyubiquitinated Proteins

In the muscle specimens of the two myotilinopathy patients, myotilin aggregates exhibited positive staining for polyubiquitin (Figure 1; see also Supplemental Figure S3 at *http://ajp.amjpathol.org*). Similarly, in electroporated mouse muscles, mMYOT aggregates were positive for polyubiquitin, and polyubiquitin-positive aggregates were more prominently observed in mMYOT S60C-expressing muscles at 14 days after electroporation. On the other hand, only few aggregates of Myc-wtMYOT were positive for polyubiquitin (Figure 6A). This result suggests that mutant myotilin was ubiquitinated or that the expressed mutant myotilin induced the deposition of polyubiquitinated proteins in the muscles of patients and electroporated mice. To characterize these aggregates, we performed a solubility assay. The muscle

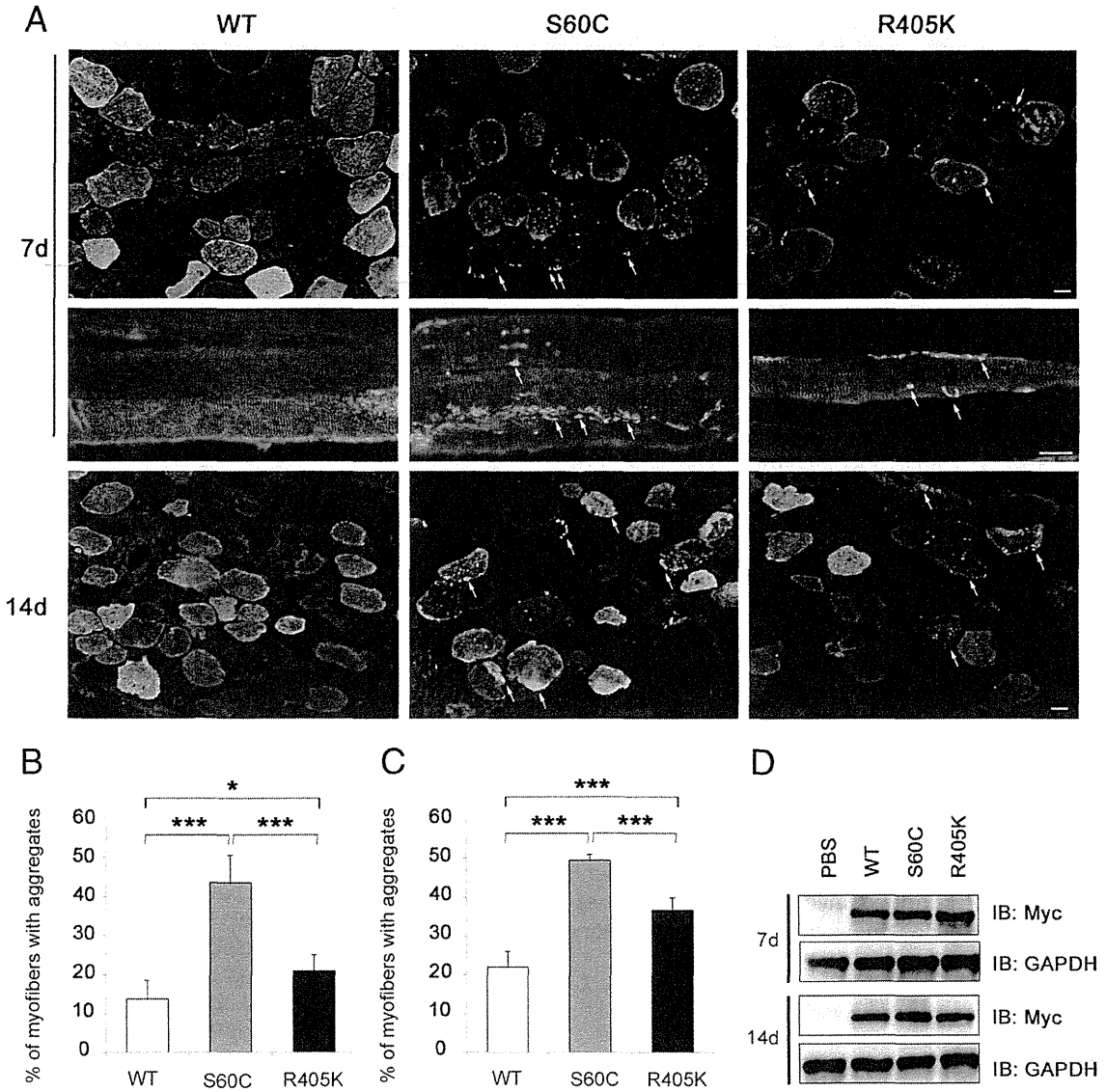

Figure 3. Enhanced aggregation of mutant myotilins in mouse skeletal muscle. **A:** Immunohistochemical staining of Myc-wtMYOT (WT)-electroporated or Myc-mMYOT (S60C or R405K)-electroporated mouse TA muscles. At 7 and 14 days after electroporation, S60C and R405K formed many Myc-positive granular aggregates (**arrows**) in myofibers, compared with WT. More prominent protein aggregates were observed in the S60C-electroporated muscle. At 14 days after electroporation, S60C-expressing myofibers exhibited larger aggregates. Scale bars: 20 μm. **B** and **C:** The percentage of myofibers with Myc-positive aggregates in the electroporated fibers of the WT, S60C, and R405K expression groups (n = 5 mice per group). $^{*}P < 0.05$; $^{***}P < 0.001$. **D:** Immunoblotting analysis of transfected Myc-tagged myotilin in 15 serial sections taken after the sections used for immunohistochemistry. GAPDH was used as a loading control.

specimen with the S60C mutation (patient 1) exhibited increased amounts of myotilin in the detergent-insoluble fraction, compared with the control specimens (Figure 6, B and D). Increasing amounts of polyubiquitinated proteins and αB-crystallin were also detected in the insoluble fraction. On the other hand, the solubilities of myotilin and other proteins, including polyubiquitin, in the muscle specimen with the R405K mutation (patient 2) were similar to those of controls (Figure 6B). Consistently, in the mouse muscles isolated at 14 days after electroporation, markedly increasing amounts of insoluble mMYOT S60C were observed (Figure 6C). In the PBS-injected control muscle, insolubility of endogenous myotilin was 31 ± 12%, whereas in the wtMYOT-, mMYOT S60C-, and mMYOT R405K-injected muscles, the Myc-tagged myotilin amounts in the insoluble fraction were 34 ± 10%, 69 ± 5%, and 48 ± 9%, respectively (Figure 6E). Insolubility of Myc-wtMYOT was similar to that of endogenous myotilin, but mMYOT, and S60C in particular, exhibited higher insolubility (Figure 6E).

These results are consistent with the number of intracellular aggregates observed after electroporation. The amount of polyubiquitinated proteins was markedly increased in the insoluble fraction of mMYOT S60C-electroporated muscles, similar to that of the muscle with the S60C mutation (patient 1) (Figure 6, B and C). A slight increase in the amount of detergent-insoluble polyubiquitinated proteins was observed in mMYOT R405K-electroporated muscles (Figure 6C). The amounts of other

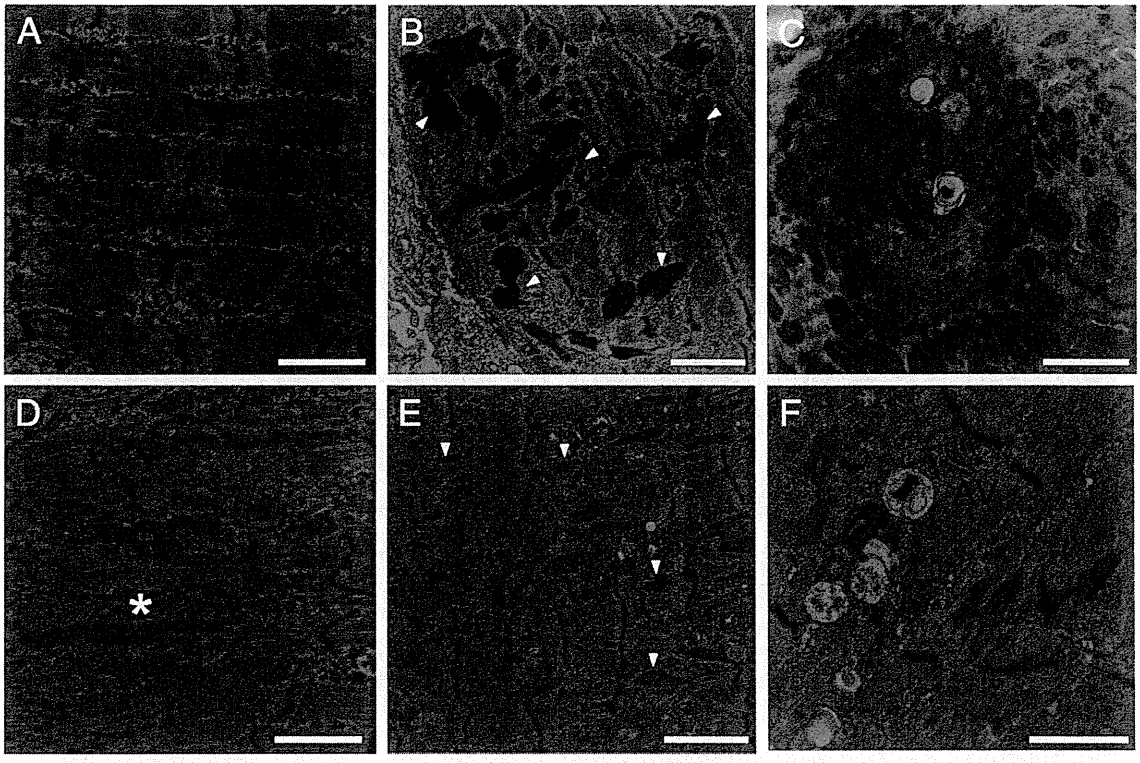

Figure 4. Electron microscopy of muscles expressing mutant myotilin. mMYOT S60C (**A–C**); mMYOT R405K (**D–F**). **A** and **D:** mMYOT-transfected muscle fibers exhibited myofibril disorganization with disrupted Z-disk; note broadening of Z-disks (**A**, **brackets**) and Z-disk streaming (**D**, **asterisk**). **B** and **E:** Variable-sized (1 to 8 μm in diameter) electron-dense inclusions (**arrowheads**) were seen in mMYOT-expressing muscles. **C** and **F:** Inclusions were occasionally associated with autophagic vacuoles (AV). **B** and **C:** Seven days after electroporation. **A** and **D–F:** Fourteen days after electroporation. Scale bars: 3.0 μm (**B** and **E**); 2.0 μm (**C**); 1.7 μm (**A** and **D**); 1.4 μm (**F**).

Z-disk–associated proteins, including αB-crystallin, in the insoluble fraction did not exhibit an increase, even in mMYOT S60C-electroporated muscles (Figure 6C; see also Supplemental Figure S4, A and B, at *http://ajp.amjpathol.org*). We also performed an immunoprecipitation assay to examine whether myotilin was polyubiquitinated. Myc-tagged myotilin proteins were immunoprecipitated from the detergent-soluble fraction of the mouse muscles isolated at 14 days after electroporation. Polyubiquitin immunoreactivity was not detected in the immunoprecipitated proteins (see Supplemental Figure S4C at *http://ajp.amjpathol.org*), indicating that neither the wt-MYOT nor the mMYOT proteins in the soluble fraction were polyubiquitinated.

Discussion

Patients with MFM, including myotilinopathy, exhibit variable clinical features. Some patients exhibit progressive weakness in proximal muscles, whereas others exhibit distal dominant muscle involvement. Cardiomyopathy, peripheral neuropathy, and respiratory insufficiency may be observed.[2] The diagnosis of MFM is generically based on characteristic pathological findings in biopsied muscles, namely, myofibrillar degradation and protein aggregation.[1] Histochemically, the most remarkable pathological changes were observed with mGT staining (Figure 1). Abnormal protein aggregates were observed, including amorphous, granular, or hyaline deposits of various sizes, shapes, and colors (dark blue, blue red, or dark green). The presence of rimmed and nonrimmed vacuoles was also a characteristic observation. Furthermore, NADH-TR staining revealed intermyofibrillar network disorganization. Attenuation or absence of NADH-TR activity in focal areas of myofibers is also observed in MFM.[1,31]

Here, we have presented findings for myotilinopathy patients with similar clinical features but different pathological changes. Fibers with cytoplasmic inclusions and disorganized myofibrils were prominent in the patient with S60C mutation, and these inclusions were strongly immunoreactive for myotilin (Figure 1).

Although transfected cultured cells did not show aggregations, our *in vivo* expression studies in mice were able to reproduce the pathological changes observed in myotilinopathy patients. Mutant myotilin caused enhanced protein aggregation in TA muscles within 1 to 2 weeks (Figure 3). The dark blue or dark green inclusions stained by mGT in mutant-expressing fibers (Figure 4) were similar to those observed in the myotilinopathy patients. Furthermore, mMYOT S60C-expressing myofibers exhibited a greater number of aggregates, which is consistent with the pathology of the patient with that mutation (patient 1). Of note, the size of mMYOT S60C aggregates markedly increased over time, suggesting that mutant myotilin may be resistant to protein degra-

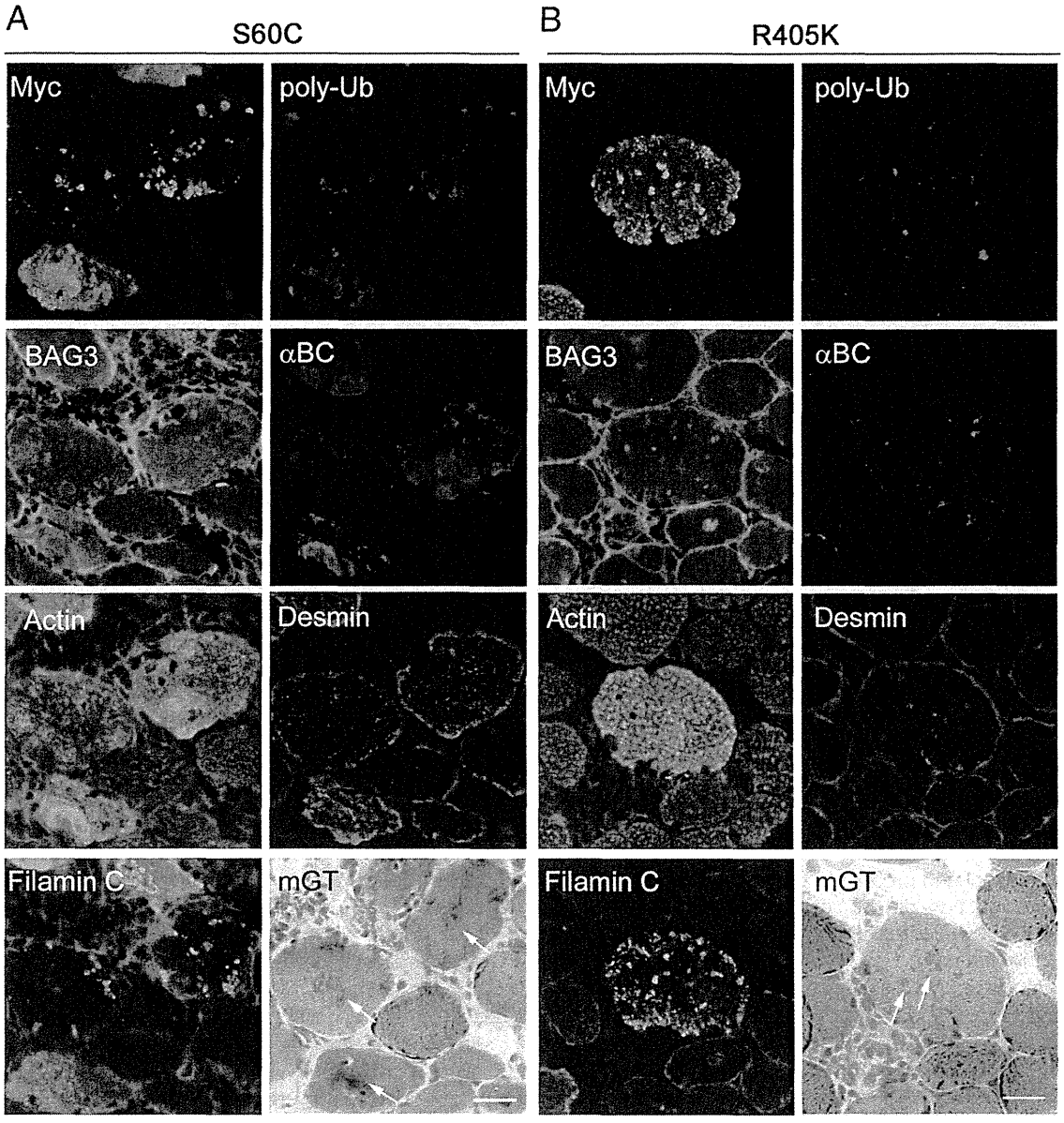

Figure 5. Mutant myotilin aggregates colocalize with polyubiquitin and other Z-disk–associated proteins in electroporated mouse muscle. mGT and immunohistochemical staining of mouse muscle expressing Myc-mMYOT S60C (**A**) or mMYOT R405K (**B**) at 14 days after electroporation. On mGT-stained sections of mMYOT-expressing muscles, cytoplasmic inclusions (**arrows**) were seen. The inclusions were immunopositive for the Myc tag in serial sections. The Myc-positive aggregates of S60C and R405K strongly colocalized with polyubiquitin (poly-Ub) and αB-crystallin (αBC). The aggregates were also immunopositive for BAG3, actin, desmin, and filamin C. Scale bars: 20 μm (**A** and **B**).

dation, as described previously for MFM-associated mutant desmin.[32,33]

Focal disorganization of myofibrils, Z-disk streaming, and accumulation of electron-dense material near the Z-disk are characteristic electron microscopic findings in the muscles of MFM patients.[17,34,35] In the myotilinopathy patient, Z-disk streaming, numerous autophagic vacuoles[17] and cytoplasmic amorphous inclusions were observed (see Supplemental Figure S2 at *http://ajp.amjpathol.org*). In the present study, expression of mMYOT by electroporation elicited myofibril disorganization and accumulation of electron-dense material, which are ultrastructural hallmarks of MFM (Figure 5). Autophagic vacuoles associated with inclusions were also observed in electroporated muscles. Disorganization of myofibrils starting from the Z-disk and material appearing to originate from the Z-disk are commonly observed in MFM patients,[34,35] and these features were also observed in the mMYOT-electroporated muscles. These morphological findings imply that the presence of mutant myotilin can induce characteristic pathological features by affecting Z-disk structure.

Ectopic accumulations of multiple proteins, including Z-disk–associated proteins, are typical pathological features of MFM.[36,37] This study and previous reports[23,38] showed that myotilin-positive protein aggregates colocal-

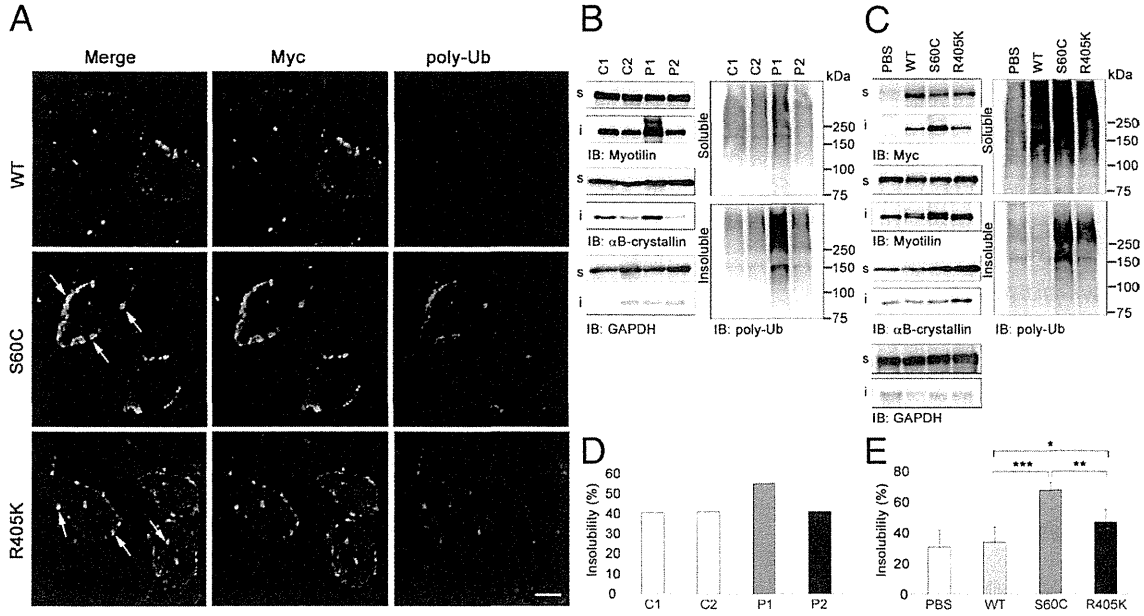

Figure 6. Mutant myotilin displays marked detergent insolubility, along with polyubiquitinated proteins. **A:** At 14 days after electroporation of Myc-wtMYOT (WT) or Myc-mMYOT (S60C or R405K), Myc-mMYOT aggregates, particularly those of S60C, colocalized with polyubiquitin (polyUb) (**arrows**). The WT aggregates rarely costained with polyubiquitin. **B–E** Solubilities of myotilin, polyubiquitinated proteins, and other sarcomeric proteins in muscles from myotilinopathy patients (**B** and **D**) and from electroporated mice (**C** and **E**). GAPDH was used as a loading control. **B:** Immunoblotting of detergent-soluble and detergent-insoluble fractions of muscles from control subjects (C1 and C2) or myotilinopathy patients [P1 (patient 1) and P2 (patient 2)]. In the muscles from P1 with S60C, markedly increasing amounts of myotilin, polyubiquitinated proteins, and αB-crystallin were detected in the insoluble fraction, compared with muscles from control subjects. **D:** Quantification of myotilin insolubilities revealed highest insolubility in P1. **C:** Immunoblotting of detergent-soluble and detergent-insoluble fractions of WT, S60C, or R405K-expressing muscles at 14 days after electroporation. Increasing amounts of insoluble Myc-tagged myotilin proteins and polyubiquitinated proteins were observed in mMYOT-electroporated muscles, compared with WT. Particularly in S60C-electroporated muscles, the amounts of insoluble proteins were notably increased. **E:** Quantification of the insolubilities of electroporated Myc-tagged myotilin in the WT, S60C, and R405K expression groups (n = 6 mice per group). Insolubility of endogenous myotilin was measured using PBS-treated mouse muscles. Compared with WT, insolubilities of electroporated Myc-tagged myotilin were significantly increased in S60C and R405K. $^{*}P < 0.05$; $^{**}P < 0.01$; $^{***}P < 0.001$. Scale bar = 20 μm.

ize with ubiquitin and Z-disk–associated proteins (ie, αB-crystallin, BAG3, actin, desmin, and filamin C) in the muscles of myotilinopathy patients (Figure 1; see also Supplemental Figure S2 at *http://ajp.amjpathol.org*). It has been reported that the myotilin T57I transgenic mice develop progressive myofibrillar changes, including Z-disk streaming and accumulation of mutant myotilin with ubiquitin and Z-disk–associated proteins, similar to those observed in myotilinopathy patients.[28] Expression of mMYOT elicited similar cytoplasmic aggregations in mouse skeletal muscle, and within 2 weeks the aggregates colocalized with polyubiquitin and other Z-disk–associated proteins. Our results indicate that mutant myotilin is able to nucleate aggregations of Z-disk–associated proteins in skeletal muscle.

MFM is a proteinopathy (ie, a protein accumulation disease). In these diseases, protein aggregates are operationally defined by poor solubility in aqueous or detergent solvents.[39,40] Such insoluble protein aggregations are characteristic of many neurodegenerative diseases.[41] In the present study, we discovered that the mutant myotilin S60C protein, along with polyubiquitinated proteins, exhibited marked detergent insolubility in muscles from both the patient and electroporated mice. Mutant myotilin R405K protein showed increased, but lower, detergent insolubility in mice (Figure 6), which may be consistent with the observation that the muscle from the patient with the R405K mutation exhibited only mild protein aggregation (Figure 1). The different detergent insolubilities exhibited by the two *MYOT* mutations may closely correlate with the amounts of protein aggregation. Here, we confirmed the aggregation-prone property of mutant myotilin, which participates in the pathogenesis of myotilinopathy. Using an immunoprecipitation assay, we also showed that electroporated mMYOT was not ubiquitinated in the detergent-soluble fraction (see Supplemental Figure S4 at *http://ajp.amjpathol.org*). A previous study showed that transfected myotilin is degraded by the proteasome system in cultured cells.[42] Our present findings show that ubiquitinated mutant myotilin can form insoluble aggregates. It is also possible that aggregation of insoluble ubiquitinated proteins is induced by the expression of mutant myotilin.

Several causative genes have been identified for MFM; however, in previous studies no mutations were found in nearly half of the MFM patients.[2] To identify the unknown causative genes, easy methods are required for determining the pathogenicity of novel mutations. Some mutant proteins exhibit protein aggregation[43–45] or biological dysfunction, including protein-protein interaction *in vitro*.[23,46–48] However, we could not detect any protein aggregation in mMYOT-expressing cultured cells (Figure 2). The difficulty of *in vitro* investigation may be responsible for the inability to identify Z-disk–associated proteins or mature Z-disk structures. Indeed, myotilin is expressed in later differentiated C2C12 myotubes with

sarcomere-like structures.[49] This suggests that mutant myotilin requires mature Z-disk and/or other sarcomeric proteins to cause aggregations. In such cases, *in vivo* examination is important for evaluating the pathogenicity of mutations. Because *in vivo* electroporation can reproduce the pathological changes observed in MFM patients within a short time, it is a useful and powerful tool for evaluating the pathogenicity of mutations in MFM.

Acknowledgments

We thank Dr. Alan H. Beggs (Children's Hospital Boston, Harvard Medical School) for the kind gift of anti-filamin C antibody and Dr. Satomi Mitsuhashi (Children's Hospital Boston, Harvard Medical School) for technical assistance in electron microscopy analysis.

References

1. Selcen D: Myofibrillar myopathies. Neuromuscul Disord 2011, 21: 161–171
2. Selcen D, Engel AG: Myofibrillar myopathy. (Updated) In GeneReviews. Copyright University of Washington, Seattle. 1997–2012. Available at http://www.ncbi.nlm.nih.gov/books/NBK1499, last revised July 27, 2010
3. OlivÉ M, Odgerel Z, Martínez A, Poza JJ, Bragado FG, Zabalza RJ, Jericó I, Gonzalez-Mera L, Shatunov A, Lee HS, Armstrong J, MaravÍ E, Arroyo MR, Pascual-Calvet J, Navarro C, Paradas C, Huerta M, Marquez F, Rivas EG, Pou A, Ferrer I, Goldfarb LG: Clinical and myopathological evaluation of early- and late-onset subtypes of myofibrillar myopathy. Neuromuscul Disord 2011, 21:533–542
4. Salmikangas P, Mykkänen OM, Grönholm M, Heiska L, Kere J, Carpén O: Myotilin, a novel sarcomeric protein with two Ig-like domains, is encoded by a candidate gene for limb-girdle muscular dystrophy. Hum Mol Genet 1999, 8:1329–1336
5. Parast MM, Otey CA: Characterization of palladin, a novel protein localized to stress fibers and cell adhesions. J Cell Biol 2000, 150: 643–656
6. Mykkänen OM, Grönholm M, Rönty M, Lalowski M, Salmikangas P, Suila H, Carpén O: Characterization of human palladin, a microfilament-associated protein. Mol Biol Cell 2001, 12:3060–3073
7. Bang ML, Mudry RE, McElhinny AS, Trombitas K, Geach AJ, Yamasaki R, Sorimachi H, Granzier H, Gregorio CC, Labeit S: Myopalladin, a novel 145-kilodalton sarcomeric protein with multiple roles in Z-disc and I-band protein assemblies. J Cell Biol 2001, 153:413–427
8. Faulkner G, Lanfranchi G, Valle G: Telethonin and other new proteins of the Z-disc of skeletal muscle. IUBMB Life 2001, 51:275–282
9. Frank D, Kuhn C, Katus HA, Frey N: The sarcomeric Z-disc: a nodal point in signalling and disease. J Mol Med (Berl) 2006, 84:446–468
10. van der Ven PF, Wiesner S, Salmikangas P, Auerbach D, Himmel M, Kempa S, Hayess K, Pacholsky D, Taivainen A, Schröder R, Carpén O, Fürst DO: Indications for a novel muscular dystrophy pathway. gamma-Filamin, the muscle-specific filamin isoform, interacts with myotilin. J Cell Biol 2000, 151:235–248
11. Gontier Y, Taivainen A, Fontao L, Sonnenberg A, van der Flier A, Carpen O, Faulkner G, Borradori L: The Z-disc proteins myotilin and FATZ-1 interact with each other and are connected to the sarcolemma via muscle-specific filamins. J Cell Sci 2005, 118:3739–3749
12. von Nandelstadh P, Ismail M, Gardin C, Suila H, Zara I, Belgrano A, Valle G, Carpen O, Faulkner G: A class III PDZ binding motif in the myotilin and FATZ families binds enigma family proteins: a common link for Z-disc myopathies. Mol Cell Biol 2009, 29:822–834
13. Witt SH, Granzier H, Witt CC, Labeit S: MURF-1 and MURF-2 target a specific subset of myofibrillar proteins redundantly: towards understanding MURF-dependent muscle ubiquitination. J Mol Biol 2005, 350:713–722
14. Salmikangas P, van der Ven PF, Lalowski M, Taivainen A, Zhao F, Suila H, Schröder R, Lappalainen P, Fürst DO, Carpén O: Myotilin, the limb-girdle muscular dystrophy 1A (LGMD1A) protein, cross-links actin filaments and controls sarcomere assembly. Hum Mol Genet 2003, 12:189–203
15. von Nandelstadh P, Grönholm M, Moza M, Lamberg A, Savilahti H, Carpén O: Actin-organising properties of the muscular dystrophy protein myotilin. Exp Cell Res 2005, 310:131–139
16. Selcen D: Myofibrillar myopathies. Curr Opin Neurol 2008, 21:585–589
17. Olivé M, Goldfarb LG, Shatunov A, Fischer D, Ferrer I: Myotilinopathy: refining the clinical and myopathological phenotype. Brain 2005, 128:2315–2326
18. Foroud T, Pankratz N, Batchman AP, Pauciulo MW, Vidal R, Miravalle L, Goebel HH, Cushman LJ, Azzarelli B, Horak H, Farlow M, Nichols WC: A mutation in myotilin causes spheroid body myopathy. Neurology 2005, 65:1936–1940
19. Hauser MA, Conde CB, Kowaljow V, Zeppa G, Taratuto AL, Torian UM, Vance J, Pericak-Vance MA, Speer MC, Rosa AL: Myotilin mutation found in second pedigree with LGMD1A. Am J Hum Genet 2002, 71:1428–1432
20. Hauser MA, Horrigan SK, Salmikangas P, Torian UM, Viles KD, Dancel R, Tim RW, Taivainen A, Bartoloni L, Gilchrist JM, Stajich JM, Gaskell PC, Gilbert JR, Vance JM, Pericak-Vance MA, Carpen O, Westbrook CA, Speer MC: Myotilin is mutated in limb girdle muscular dystrophy 1A. Hum Mol Genet 2000, 9:2141–2147
21. Penisson-Besnier I, Talvinen K, Dumez C, Vihola A, Dubas F, Fardeau M, Hackman P, Carpen O, Udd B: Myotilinopathy in a family with late onset myopathy. Neuromuscul Disord 2006, 16:427–431
22. Berciano J, Gallardo E, Dominguez-Perles R, Garcia A, Garcia-Barredo R, Combarros O, Infante J, Illa I: Autosomal-dominant distal myopathy with a myotilin S55F mutation: sorting out the phenotype. J Neurol Neurosurg Psychiatry 2008, 79:205–208
23. Shalaby S, Mitsuhashi H, Matsuda C, Minami N, Noguchi S, Nonaka I, Nishino I, Hayashi YK: Defective myotilin homodimerization caused by a novel mutation in MYOT exon 9 in the first Japanese limb girdle muscular dystrophy 1A patient. J Neuropathol Exp Neurol 2009, 68:701–707
24. Reilich P, Krause S, Schramm N, Klutzny U, Bulst S, Zehetmayer B, Schneiderat P, Walter MC, Schoser B, Lochmüller H: A novel mutation in the myotilin gene (MYOT) causes a severe form of limb girdle muscular dystrophy 1A (LGMD1A). J Neurol 2011, 258:1437–1444
25. Mavroidis M, Panagopoulou P, Kostavasili I, Weisleder N, Capetanaki Y: A missense mutation in desmin tail domain linked to human dilated cardiomyopathy promotes cleavage of the head domain and abolishes its Z-disc localization. FASEB J 2008, 22:3318–3327
26. Wang X, Osinska H, Klevitsky R, Gerdes AM, Nieman M, Lorenz J, Hewett T, Robbins J: Expression of R120G-alphaB-crystallin causes aberrant desmin and alphaB-crystallin aggregation and cardiomyopathy in mice. Circ Res 2001, 89:84–91
27. Wang X, Osinska H, Dorn GW 2nd, Nieman M, Lorenz JN, Gerdes AM, Witt S, Kimball T, Gulick J, Robbins J: Mouse model of desmin-related cardiomyopathy. Circulation 2001, 103:2402–2407
28. Garvey SM, Miller SE, Claflin DR, Faulkner JA, Hauser MA: Transgenic mice expressing the myotilin T57I mutation unite the pathology associated with LGMD1A and MFM. Hum Mol Genet 2006, 15:2348–2362
29. Hayashi YK, Matsuda C, Ogawa M, Goto K, Tominaga K, Mitsuhashi S, Park YE, Nonaka I, Hino-Fukuyo N, Haginoya K, Sugano H, Nishino I: Human PTRF mutations cause secondary deficiency of caveolins resulting in muscular dystrophy with generalized lipodystrophy. J Clin Invest 2009, 119:2623–2633
30. Thompson TG, Chan YM, Hack AA, Brosius M, Rajala M, Lidov HG, McNally EM, Watkins S, Kunkel LM: Filamin 2 (FLN2): A muscle-specific sarcoglycan interacting protein. J Cell Biol 2000, 148:115–126
31. Schröder R, Schoser B: Myofibrillar myopathies: a clinical and myopathological guide. Brain Pathol 2009, 19:483–492
32. Liu J, Chen Q, Huang W, Horak KM, Zheng H, Mestril R, Wang X: Impairment of the ubiquitin-proteasome system in desminopathy mouse hearts. FASEB J 2006, 20:362–364
33. Liu J, Tang M, Mestril R, Wang X: Aberrant protein aggregation is essential for a mutant desmin to impair the proteolytic function of the ubiquitin-proteasome system in cardiomyocytes. J Mol Cell Cardiol 2006, 40:451–454
34. Selcen D, Ohno K, Engel AG: Myofibrillar myopathy: clinical, morphological and genetic studies in 63 patients. Brain 2004, 127:439–451

35. Claeys KG, Fardeau M, Schröder R, Suominen T, Tolksdorf K, Behin A, Dubourg O, Eymard B, Maisonobe T, Stojkovic T, Faulkner G, Richard P, Vicart P, Udd B, Voit T, Stoltenburg G: Electron microscopy in myofibrillar myopathies reveals clues to the mutated gene. Neuromuscul Disord 2008, 18:656–666
36. Claeys KG, van der Ven PF, Behin A, Stojkovic T, Eymard B, Dubourg O, Laforêt P, Faulkner G, Richard P, Vicart P, Romero NB, Stoltenburg G, Udd B, Fardeau M, Voit T, Fürst DO: Differential involvement of sarcomeric proteins in myofibrillar myopathies: a morphological and immunohistochemical study. Acta Neuropathol 2009, 117:293–307
37. Olivé M: Extralysosomal protein degradation in myofibrillar myopathies. Brain Pathol 2009, 19:507–515
38. Janué A, Olivé M, Ferrer I: Oxidative stress in desminopathies and myotilinopathies: a link between oxidative damage and abnormal protein aggregation. Brain Pathol 2007, 17:377–388
39. Fink AL: Protein aggregation: folding aggregates, inclusion bodies and amyloid. Fold Des 1998, 3:R9–R23
40. Kopito RR: Aggresomes, inclusion bodies and protein aggregation. Trends Cell Biol 2000, 10:524–530
41. Ross CA, Poirier MA: Protein aggregation and neurodegenerative disease. Nat Med 2004, 10:S10–S17
42. von Nandelstadh P, Soliymani R, Baumann M, Carpen O: Analysis of myotilin turnover provides mechanistic insight into the role of myotilinopathy-causing mutations. Biochem J 2011, 436:113–121
43. Goldfarb LG, Vicart P, Goebel HH, Dalakas MC: Desmin myopathy. Brain 2004, 127:723–734
44. Vicart P, Caron A, Guicheney P, Li Z, Prévost MC, Faure A, Chateau D, Chapon F, Tomé F, Dupret JM, Paulin D, Fardeau M: A missense mutation in the alphaB-crystallin chaperone gene causes a desmin-related myopathy. Nat Genet 1998, 20:92–95
45. Selcen D, Muntoni F, Burton BK, Pegoraro E, Sewry C, Bite AV, Engel AG: Mutation in BAG3 causes severe dominant childhood muscular dystrophy. Ann Neurol 2009, 65:83–89
46. Sharma S, Mücke N, Katus HA, Herrmann H, Bär H: Disease mutations in the "head" domain of the extra-sarcomeric protein desmin distinctly alter its assembly and network-forming properties. J Mol Med (Berl) 2009, 87:1207–1219
47. Bär H, Kostareva A, Sjöberg G, Sejersen T, Katus HA, Herrmann H: Forced expression of desmin and desmin mutants in cultured cells: impact of myopathic missense mutations in the central coiled-coil domain on network formation. Exp Cell Res 2006, 312:1554–1565
48. Bova MP, Yaron O, Huang Q, Ding L, Haley DA, Stewart PL, Horwitz J: Mutation R120G in alphaB-crystallin, which is linked to a desmin-related myopathy, results in an irregular structure and defective chaperone-like function. Proc Natl Acad Sci USA 1999, 96:6137–6142
49. Mologni L, Moza M, Lalowski MM, Carpén O: Characterization of mouse myotilin and its promoter. Biochem Biophys Res Commun 2005, 329:1001–1009

Neuroscience Research 72 (2012) 181–186

Contents lists available at SciVerse ScienceDirect

Neuroscience Research

journal homepage: www.elsevier.com/locate/neures

Continuous administration of poloxamer 188 reduces overload-induced muscular atrophy in dysferlin-deficient SJL mice

Naoki Suzuki[a,*], Tetsuya Akiyama[a], Toshiaki Takahashi[b], Hazuki Komuro[a], Hitoshi Warita[a], Maki Tateyama[a], Yasuto Itoyama[c], Masashi Aoki[a]

[a] Department of Neurology, Tohoku University School of Medicine, 1-1 Seiryo-machi, Aoba-ku, Sendai, Japan
[b] Department of Neurology, National Nishitaga Hospital, Sendai, Japan
[c] National Center Hospital, National Center of Neurology and Psychiatry (NCNP), Tokyo, Japan

ARTICLE INFO

Article history:
Received 28 May 2011
Received in revised form 3 October 2011
Accepted 4 October 2011
Available online 21 October 2011

Keywords:
Dysferlinopathy
Muscular dystrophy
Poloxamer 188 (P188)
Osmotic pump
p38
Atrogin-1

ABSTRACT

Dysferlin-deficient SJL mice are commonly used to study dysferlinopathy. We demonstrated that poloxamer 188 (P188), a membrane sealant, is effective in reducing the loss of muscle mass in SJL mice when administered using an osmotic pump for 6 weeks. We did not observe significant changes over a 2-week administration period, suggesting that longthier observation is necessary to determine the effectiveness of P188. We also examined exercise endurance in P188-administered SJL mice using a rolling cage. Phosphorylated p38 was found to be reduced in P188-administered SJL mice; additionally, using microarray analysis, we found diminished expression of atrogin-1, an E3 ubiquitin ligase, as the effector of muscular atrophy. Chronic infusion of P188 to dysferlin-deficient SJL mice reduced muscular atrophy, and administering p38 and atrogin-1 in the gastrocnemius muscle improved its motor function. These results provide a basis for potential treatments for dysferlin-deficient skeletal muscle fibers.

1. Introduction

Mutations in the dysferlin gene cause several phenotypes of muscular dystrophy, called "dysferlinopathies"; these include limb-girdle muscular dystrophy type 2B (LGMD2B), Miyoshi myopathy (MM), and distal anterior compartment myopathy (DACM) (Aoki et al., 2001; Bashir et al., 1998; Illa et al., 2001; Klinge et al., 2010; Liu et al., 1998; Paradas et al., 2010; Rosales et al., 2010; Takahashi et al., 2003). Dysferlinopathies are autosomal recessive diseases, and different phenotypes are observed even within the same family (Illarioshkin et al., 2000; Saito et al., 2007). Dysferlin deficiency has been proven to lead to defective membrane resealing in skeletal muscle and muscle necrosis (Bansal et al., 2003).

SJL mice, which display dysferlin deficiencies (Bittner et al., 1999) and inflammatory muscle changes (Suzuki et al., 2005), are commonly used to study dysferlinopathy. The spontaneous myopathy of SJL mice begins at 4–6 weeks of age and is nearly complete by eight months of age. The mutation in SJL mice is an in-frame deletion of 171 base pairs of the dysferlin gene. Assuming that the structure of the gene is similar in mice and humans, this in-frame deletion predicts that in human mutations 57 amino acids of dysferlin protein, including most of the fourth C2 domain, would be absent.

Poloxamer 188 (P188) is a stable 8.4 kDa amphiphilic polymer that localizes in lipid monolayers (Wu et al., 2005) and damaged regions of membranes (Maskarinec et al., 2005). When applied to injured cells, P188 repairs disrupted membranes and enhances the recovery of skeletal muscle (Lee et al., 1992), fibroblasts (Merchant et al., 1998), and the spinal cord (Borgens et al., 2004) following a variety of injury-inducing protocols. Chemically based membrane sealants have been acutely tested in mdx mice and have recently been proposed as a new therapeutic approach for cardiac membrane stabilization in muscular dystrophy (Yasuda et al., 2005). This treatment modality aims to directly seal the membrane tears that occur in the absence of dystrophin. Cases of Duchenne muscular dystrophy (DMD) in mdx mice showed that application of the membrane sealant poloxamer 188 (P188) confers acute cardiac protection. Additionally, the chronic infusion of severely affected dystrophic dogs with membrane-sealing poloxamer reduced myocardial fibrosis and fully prevented left ventricular remodeling (Townsend et al., 2010). The effects of P188 on other types of muscular dystrophy have not been examined.

Our aim was to determine the effects of P188 when administered with an osmotic pump for 6 weeks in a mouse model of dysferlinopathy. Using SJL mice, we found that p38 and atrogin-1 played

* Corresponding author. Tel.: +81 22 717 7189; fax: +81 22 717 7192.
E-mail address: naoki@med.tohoku.ac.jp (N. Suzuki).

0168-0102/$ – see front matter © 2011 Elsevier Ireland Ltd and the Japan Neuroscience Society. All rights reserved.
doi:10.1016/j.neures.2011.10.005

key roles in the influence of P188 on the progression of muscular atrophy induced by overloading.

2. Materials and methods

2.1. Animals

All mice were handled according to approved animal protocols in our institution. Gastrocnemius and tibialis anterior muscles were dissected from female control mice (SWR) and SJL (SJL/JOrllcoCrj) mice (Charles River Japan Inc., Yokohama, Japan) ($n = 10$ and 50, respectively). Prior to this study, we had examined the muscles of both strains of mice to investigate the muscular pathology and progression of myopathy (Suzuki et al., 2005). In 2-month-old SJL mice, there were slight or no muscle changes compared with the control mice. In contrast, 9-month-old SJL mice had an increased variety of fiber diameters, degenerating fibers, regenerating fibers, and increased inflammatory responses. With those results in mind, mice within the 19- to 25-week age range were chosen for use.

2.2. Creatine kinase (CK) determination

Blood (200 μL) was collected in Eppendorf tubes using cardiac puncture under deep anesthesia and allowed to clot at room temperature prior to centrifugation and serum collection. CK determination was performed according to the manufacturer's instructions using a standard spectrophotometric method. The data were expressed as units per liter.

2.3. Reagents and osmotic pump

19-Week-old mice were operated upon. Sterile saline was injected into the control mice. The total dose of poloxamer 188 (P188; Sigma–Aldrich, MO) was 20 mg, infused continuously for 42 days. The dosage was modified from that used in previous reports (Ng et al., 2008; Quinlan et al., 2006; Yasuda et al., 2005). The osmotic pumps (Alzet osmotic pump 2006, Alzet, CA) were incubated in sterile saline at 37 °C for 40 h to attain a constant flow rate prior to use. The pumps were filled to capacity with either P188 or sterile saline using a filling needle. SJL and SWR mice (19 weeks old) were anesthetized using intraperitoneal Nembutal. The skin between the scapulas was incised, and the pumps were implanted in the subcutaneous pocket. The normal pumping rate was 0.15 μL/h for 6 weeks. The reservoir volume was 200 μL, and the weight of each osmotic pump was 1.1 g. The mice were sampled at 25 weeks old, with body weights between 25 and 30 g.

2.4. Functional tests

Grip strength of the forearms was assessed using a grip strength meter (GPM-100, MelQuest, Japan) according to the manufacturer's instructions. 25-Week-old mice were used. Three successful forelimb strength measurements ($n = 5$) were recorded in the morning by an investigator blinded to treatment conditions. The average grip strength measurement from each day was used for the subsequent analysis. Motor endurance was measured using a rolling cage (RS-204-5, Kori-Seiki, Japan). The number of rotations per day was recorded, and the average number of rotations for three consecutive days was calculated ($n = 5$).

2.5. Tissue preparation

Both body and wet muscle weight were recorded. The gastrocnemius and tibialis anterior muscles were collected individually using standard dissection methods and cleaned of excess fat, connective tissue, and tendons. Several of the muscles were frozen in isopentane that was cooled by liquid nitrogen for histological and immunohistochemical analysis, whereas the other muscles were frozen directly in liquid nitrogen for either RNA isolation or protein extraction and stored at −80 °C.

2.6. RNA extraction

RNA was extracted from the gastrocnemius, tibialis anterior, and soleus muscles using Qiagen RNeasy Fibrous Tissue Mini Kits (Qiagen, CA). RNA concentrations were determined using a spectrophotometer, and the RNA quality was assessed using an Agilent 2100 Bioanalyzer (Agilent Technologies, CA). All RNA samples had RNA Integrity Numbers (RIN) of 9.0 or higher.

2.7. Real time PCR

For RT-PCR, first strand cDNA was synthesized using oligo-dT primers. The expression levels of selected genes (atrogin-1/MAFbx and beta-actin) were analyzed using CFX96 (BioRad, CA) following the manufacturer's instructions. The primers were 5′-TCGCAGCCAAGAAGAGAAAG-3′, 5′-GGCAGTCGAGAAGTCCAGTC-3′ for atrogin-1 and 5′-CTGGCTCCTAGCACCATGAAGAT-3′, 5′-GGTGGACAGTGAGGCCAGGAT-3′ for beta-actin.

2.8. Western blotting

Skeletal muscle protein was extracted from mouse hindlimb muscle samples for Western blot analysis. We used the Bradford method and Coomassie Brilliant Blue G-250 (Bio-Rad) to determine the protein concentrations. Protein fractions were then extracted using a reducing sample buffer containing 10% SDS, 70 mM Tris–HCl, 5% β-mercaptoethanol and complete inhibitor cocktail (Roche, Basel, Swiss). Protein (15 or 30 μg per lane) was separated on a SDS-polyacrylamide gel, and the resulting gel was subsequently transferred to a polyvinylidene difluoride membrane (Millipore) using 250 mA for 1 h. The blot was later incubated with the primary antibodies. The signals were detected using the enhanced chemiluminescence plus method (GE, NJ). Relative quantities of proteins in the western blots were determined using scanning densitometry and expressed in arbitrary units.

2.9. Nuclear fractionation

2.9.1. Nuclear and cytosolic protein extraction

Nuclear extracts were taken from mouse skeletal muscle as previously described (Suzuki et al., 2007). The cytosolic extract was obtained from the first supernatant of the nuclear extract preparation. The supernatant was placed in Millipore Ultrafree-4 centrifugal columns that had been pre-wetted with 0.5 mL of dilution buffer (20 mM HEPES, 40 mM KCl, 10% glycerol, 0.2 mM EDTA, 1 mM DTT) and centrifuged (7500 × g) at 4 °C for 30 min. Dilution buffer (0.8 mL) was added to the column, and the 30-min spin was repeated.

2.10. Statistical analysis

Significant differences were determined with either the unpaired Student's t-test or the Mann–Whitney test using Excel. All data are expressed as the means ± SEM. Statistical significance is defined as $^*p < 0.05$.